Department of Physics and Astronomy
Heidelberg University

Bachelor Thesis in Physics
submitted by

Daniel Di Marco

born in Spaichingen (Germany)

2024

Characterisation of a Raspberry Pi NoIR v2 camera module for monitoring the beam shape and position of a 2 kW laser in the CSR system

This Bachelor Thesis has been carried out by Daniel Di Marco at the
Max Plank Institute for Nuclear Physics in Heidelberg
under the supervision of
PD. Dr. Holger Kreckel
and
Apl. Prof. Dr. Ulrich Schmidt

Monitoring the shape and position of a 2 kW laser beam profile with a Raspberry Pi NoIR v2 camera module:

At the Cryogenic Storage Ring (CSR) at the Max Planck Institute for Nuclear Physics in Heidelberg, collisions between neutral particles and ions can be studied at temperatures as low as (5.5 ± 1.0) K . Neutral particles are generated through photodetachment of a negative ion beam using a 2 kW laser diode system at 808 nm. This laser operates in either continuous wave (cw) or pulsed mode and its power is measured with a power meter. To monitor the beam position and shape in both cw and pulsed modes on the power meter, we characterized the working regime of a Raspberry Pi NoIR v2 camera module in a test setup with a 15 mW laser at 650 nm. Additionally, we estimated the necessary filters to avoid saturation on the camera for both the 15 mW and 2 kW lasers. The laser beam shape of a 10 mW laser diode at 650 nm was measured using the knife-edge technique, and the results agreed within errors with those obtained from the camera.

Überwachung der Form und Position eines 2kW-Laserstrahlprofils mit einem Raspberry Pi NoIR v2 Kameramodul:

Am Kryogenen Speicherring (CSR) am Max-Planck-Institut für Kernphysik in Heidelberg können Kollisionen zwischen neutralen Teilchen und Ionen bei Temperaturen von bis zu $(5,5 \pm 1,0)$ K untersucht werden.[1] Neutrale Teilchen werden durch Photodetachment eines negativen Ionenstrahls mit einem 2 kW Diodenlaser bei 808 nm erzeugt. Dieser Laser arbeitet entweder im kontinuierlichen (cw) oder im gepulsten Modus und wird mit einem Leistungsmesser überwacht. Um die Position und die Form des Strahls sowohl im cw- als auch im gepulsten Modus auf dem Leistungsmesser zu überwachen, haben wir das Arbeitsregime eines Raspberry Pi NoIR v2 Kameramoduls in einem Testaufbau mit einem 15 mW-Laser bei 650 nm charakterisiert. Außerdem haben wir die erforderlichen Filter zur Vermeidung von Sättigung der Kamera sowohl für den 15 mW- als auch für den 2 kW-Laser abgeschätzt. Die Form des Laserstrahls einer 10-mW-Laserdiode bei 650 nm wurde mit der Messerschneidetechnik gemessen, und die Ergebnisse stimmten innerhalb der Fehlergrenzen mit denen der Kamera überein.

Contents

List of Figures

List of Tables

1 Motivation

At the Max Planck Institute for Nuclear Physics in Heidelberg experiments on ion-neutral merged beams are studied in a cryogenic storage ring (CSR) at temperatures as low as (5.5±1.0) K.[1,2] The neutral beam is produced by neutralisation of a negative ion beam, in which a laser strips off the outer electron via photodetachment for a fraction of the ions.[3] The laser system was manufactured by DILAS Inc. and consists of two vertical stacks containing 15 bars. Each bar also consists of 19 individual diode emitters. This construction results in a matrix of 30x19 individual beamlets, which are collimated with mirco-optical lenses and are further shaped by several optical elements as illustrated in figure 1.[4] Beyond the focus, the profile of the laser can be modelled as a Gaussian beam with a gaussian-quality-factor $M^2 \approx 100$. In the near-field however, the laser profile appears box-like.[4] The laser operates in the near-infrared regime with a wavelength of 808 nm and is capable of producing up to 2 kW of power in continuous wavemode.[3] However, for most experiments the laser is operated in pulsed mode.

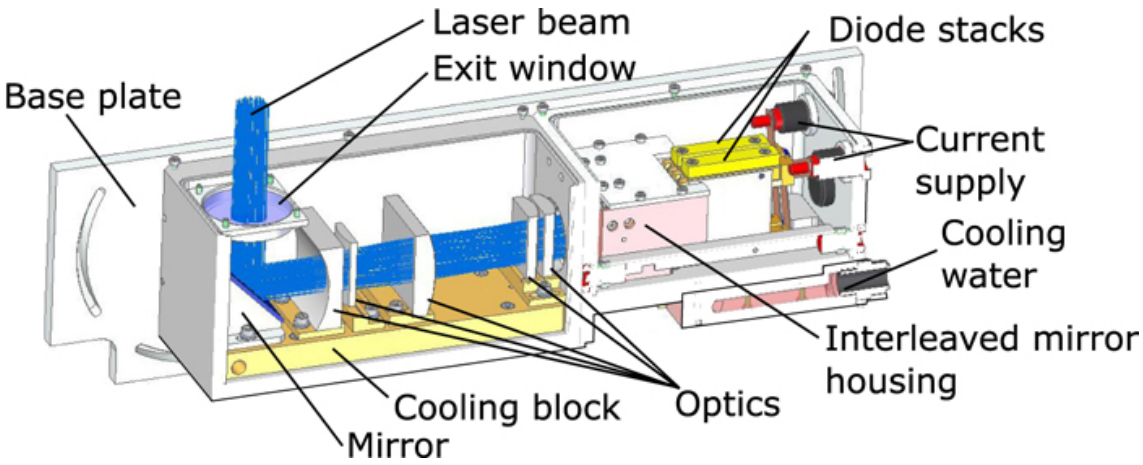

Figure 1: Illustration of the laser diode system used for creation of neutral beams for the CSR experiments at the Max Planck Institute for Nuclear Physics.[4]

The neutralisation process of the negative ion beam happens inside a closed box, i.e. the photodetachment chamber, which consists of two laser boxes connected by a drift tube. An overview is given in figure 2. The ion beam is overlapped with the laser beam at an angle of $\theta = 2.7°$ inside of the drift tube.[3] While the ion/neutral beam leaves the photodetachment box through the second aperture and enters afterwards the CSR, the laser beam enters a small area inside of the second laser box through the laser window on the right-hand-side of the drift tube and is reflected onto a water-cooled power meter (Coherent Power-head PM3K).[4] Where the optical power of the laser is thermally measured in the range of (0.1-3) kW with a resolution of 1 W.[5]

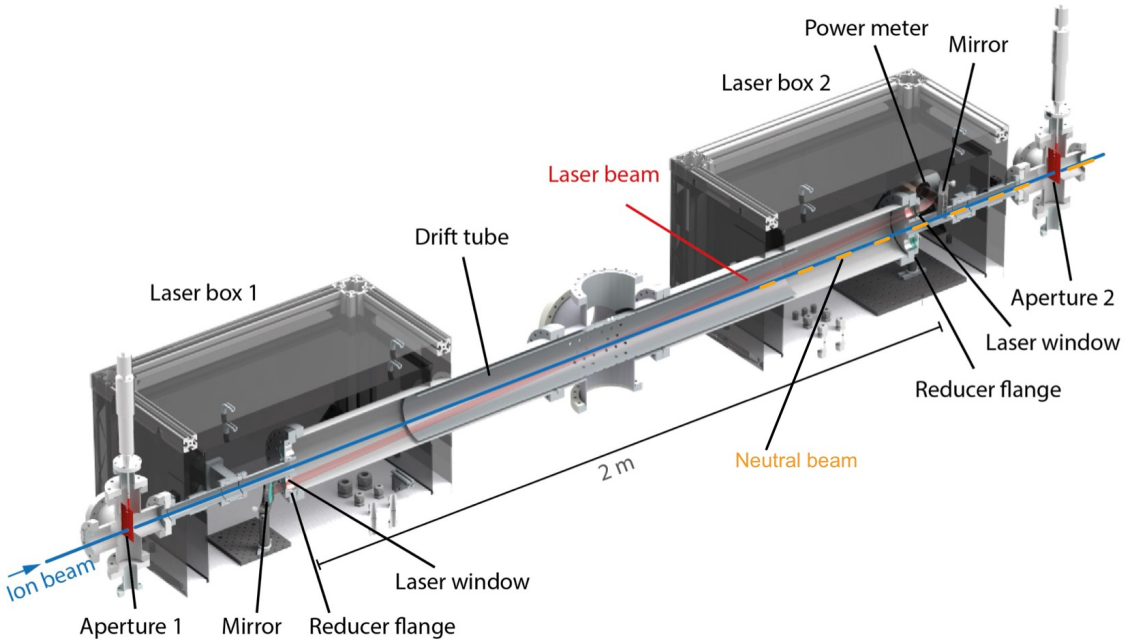

Figure 2: Cross section of the photodetachment chamber. The 2 kW laser system is on the side next to the box which is cut off in the cross section.[3]

For the last ten years the laser system needed very little maintenance, besides occasional realignment procedures every couple of years, which were indicated by smaller power values measured over time. After realignment however, the total laser power could mostly have been recovered.

In December 2023, a reproducible error occurred in which the laser turned off when the laser power was increased too fast. During a check of the alignment we had the impression that the shape of the laser beam had changed. In order to avoid such problems in the future, we would like to establish a method to monitor the shape and position of the laser beam during experiments. The aim of this thesis is to find and characterize a camera for this purpose. For safety reasons when handling a 2 kW laser, the camera was characterised with an external setup that includes a laser diode at 650 nm and optical output powers of up to 15 mW. This optical setup allows us to make quick changes to the test-setup and is therefore easier to handle. The intensities on the camera should be comparable if an OD filter is used in the CSR setup that is at least 5 orders of magnitude stronger than in the test setup. This is because the test setup laser and the 2 kW laser differ by about 5 orders of magnitude in power. We chose to use reflective optical density (OD) filters, since even a small reflection of the 2 kW beam could consist of considerable power that can heat up the filters.

2 Principles of laser physics

In this chapter we give a short introduction to laser physics and especially laser diodes, since they are used in this thesis.

2.1 Interaction of light and matter

2.1.1 Quantum optical processes

At the beginning of the 20th century, the interaction between light and matter was not yet fully understood. The process of absorption had already been described mathematically, but spontaneous emission had only been observed in experiments. It was Albert Einstein, who put these two processes into a coherent mathematical framework in his work "On the Quantum Theory of Radiation" published in 1916.[6] Within the framework of these two processes, he also described another possible type of interaction, which he called stimulated emission.[6] For the mathematical description an atom is assumed to be in a radiation field. The eigenstates of the atom are given by $|k\rangle$ ($k \in \mathbb{N}$) with energies E_k and the spectral energy density of the radiation field $\omega(\nu) = n(\nu) \cdot h \cdot \nu$. With $n(\nu)$ counting the number of photons with frequency ν and Plank's constant h. Therefore, the energy of a photon with frequency ν is $E_\gamma(\nu) = h \cdot \nu$.[7]

Absorption:
In the process of stimulated absorption, the atom absorbs a photon of energy E_γ from the radiation field and gets excited into a higher state. The energy of the excited atom is given by $E_f = E_i + E_\gamma(\nu)$, where i and f denote initial and final state.[7] The number of photons with frequency ν of the radiation field decreases by one. The probability $W^{abs}_{n\to m}$ of this process with involving atom states $|n\rangle$ and $|m\rangle$ ($n < m$), depends on the spectral energy density of the radiation field $\omega(\nu)$. The proportionality factor is called the Einstein coefficient for absorption $B_{n\to m}$.[7] The probability is given in equation 1.

$$W^{abs}_{n\to m} = B_{n\to m} \cdot \omega(\nu) \tag{1}$$

The process is visualized in figure 3.

Stimulated emission:
The process of stimulated emission describes the emission of a photon of energy $\Delta E = E_m - E_n$ as an atom transitions from an excited energy state $|m\rangle$ into a lower state $|n\rangle$. The process is induced by an initial photon whose energy matches the energy difference of the two states, e.g. $E_\gamma(\nu) = \Delta E$.[7] This process emits a real duplicate of the initial photon, i.e. both posses the same characteristics like direction of traveling, phase and polarisation.[8] Thus the number of photons with frequency ν of the radiation field increases by one. Like the process of absorption, the probability $W^{st.\ em.}_{m\to n}$ of stimulated emission to occur depends on the spectral energy density $\omega(\nu)$. The constant of proportionality is the associated Einstein coefficient of stimulated emission, i.e. $B_{m\to n}$.[7] The probability of this process is given in equation 2.

$$W^{st.\ em.}_{m\to n} = B_{m\to n} \cdot \omega(\nu) \tag{2}$$

The process is shown in figure 3.

Spontaneous emission:
Spontaneous emission describes the transition of an atom from an excited energy state $|m\rangle$ into a lower state $|n\rangle$. This process also emits a photon of the energy $\Delta E = E_m - E_n$.[7] However, this process is not induced by an initial photon but spontaneous. The emitted photon has random

direction of travel, phase and polarization. The number of photons from the radiation field with the same frequency increases again by one.[8] Unlike the other two processes the probability for spontaneous emission $W_{m\to n}^{sp.\ em.}$ does not rely on the radiation field and is therefore independent of the spectral energy density $\omega(\nu)$.[8] This probability is also known as the Einstein coefficient of spontaneous emission $A_{m\to n}$ as shown in equation 3.[7]

$$W_{m\to n}^{sp.\ em.} = A_{m\to n} \tag{3}$$

The process is shown in figure 3.

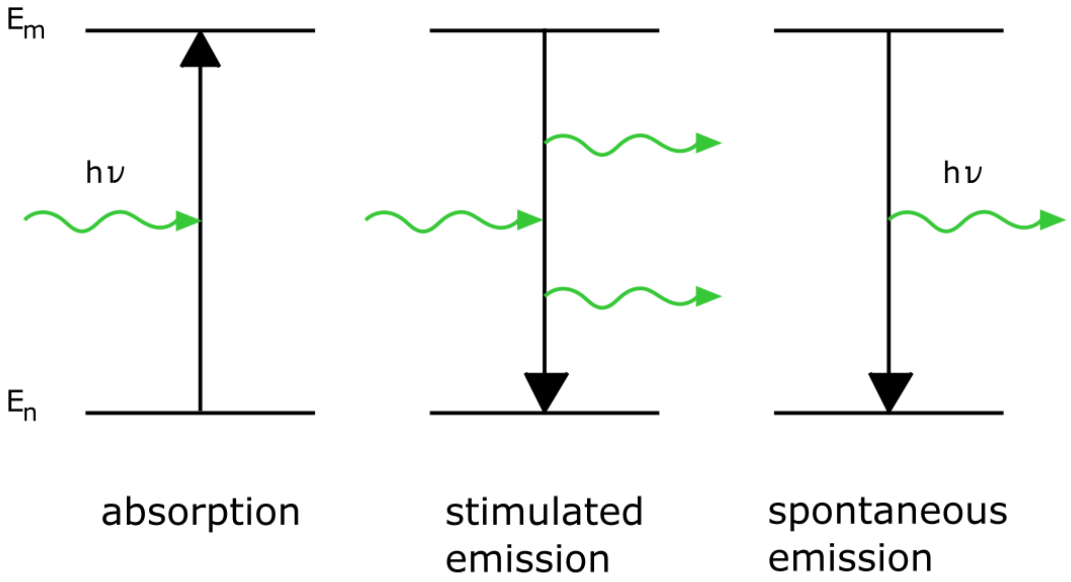

Figure 3: Visualization of the three quantum optical processes.[9]

2.1.2 Einstein coefficients

To derive a relation between the different Einstein coefficients, we assume that several atoms of one species with energy states $|m\rangle$ and $|n\rangle$ are in a radiation field. The number of atoms N_k in an arbitrary state $|k\rangle$ can be described via the Boltzmann distribution as shown in equation 4.

$$N_k = g_k e^{-\beta E_k} \qquad \beta = \frac{1}{k_B T} \tag{4}$$

Here, g_k denotes the degeneracy of the state $|k\rangle$ and k_B is the Boltzmann constant. In a case of steady state equilibrium, the ratio $\frac{N_m}{N_n}$ of the atoms in the sates $|m\rangle$ and $|n\rangle$ has to be constant over time.[7] Therefore, the three types of interaction between the atoms and the radiation field have to balance each other out. This is described by equation 5.[7]

$$A_{m\to n}N_m + B_{m\to n}\omega(\nu)N_m = B_{n\to m}\omega(\nu)N_n \tag{5}$$

Here the first term of the left-hand-side describes the occurrence of spontaneous emission and the second term the occurrence of stimulated emission. The term on the right-hand-side denotes

the amount of absorption processes. Using equation 4 for the numbers N_m, N_n for the atoms in the states $|m\rangle$, $|n\rangle$ in equation 5 and solving for $\omega(\nu)$ yields:

$$\omega(\nu) = \left[\frac{A_{m\to n}}{B_{m\to n}}\right] \cdot \frac{1}{(\frac{g_n B_{n\to m}}{g_m B_{m\to n}})e^{\beta(E_n - E_m)} - 1} \tag{6}$$

A comparison to Planck's radiation law (equation 7)[7] leads to the relations shown in equation 8 and 9.

$$\rho(\nu) = \left[\frac{8\pi\nu^2}{c^3}\right] [h\nu] \frac{1}{e^{\beta \cdot h\nu} - 1} \tag{7}$$

Here, c denotes the speed of light and the last term represents the photon population $n(\nu)$.

$$g_m B_{m\to n} = g_n B_{n\to m} \tag{8}$$

$$\frac{A_{m\to n}}{B_{m\to n}} = \frac{8\pi\nu^2}{c^3} \cdot h\nu \tag{9}$$

The first relation describes the ratio of probabilities for absorption and stimulated emission, while taking into account the degeneracy of the energy states.[7] The second relation shows that the probability for spontaneous emission is proportional to stimulated emission. Furthermore, this derivation shows that Planck's radiation law is based on a balance of the three types of interactions.[9]

2.2 The laser effect

2.2.1 Amplification of light

The system introduced in chapter 2.1.2 can be used to amplify coherent light if the number of occurring stimulated emission processes $W^{st.\ em.}_{m\to n} \cdot N_m$ dominates the number of absorption processes $W^{abs.}_{n\to m} \cdot N_n$.[9] For the system in thermal equilibrium the ratio is given in equation 10.

$$\frac{W^{st.\ em.}_{m\to n} N_m}{W^{abs.}_{n\to m} N_n} = \frac{B_{m\to n} N_m}{B_{n\to} N_n} \overset{(8)}{=} \frac{g_n N_n}{g_m N_n} = e^{-\beta(E_m - E_n)} < 1 \tag{10}$$

Therefore, absorption dominates stimulated emission and light is attenuated, if the system is in thermal equilibrium. To give an example, the relation in occupation numbers N_2 and N_1 for two fictitious energy states $|2\rangle$, $|1\rangle$ with degeneracies $g_2 = 3$, $g_1 = 1$ for a typical energy scale of $E_2 - E_1 = 1eV$ is:[9]

$$\frac{N_2}{N_1} = \frac{g_2}{g_1} e^{-\beta(E_2 - E_1)} \approx 3 \cdot 10^{-18} << 1 \tag{11}$$

In order to amplify coherent light, the system must be brought out of thermal equilibrium.[10] This might be done by an energy-pump which inserts energy into the system, such that $\frac{g_2 N_1}{g_1 N_2} >> 1$. This is known as a population inversion and the general case is described by equation 12.[7]

$$\frac{g_m N_n}{g_n N_m} > 1 \tag{12}$$

A population inversion describes the case in which more atoms of the medium reside in higher energy states.[10] Equation 12 considers the degeneracies of the energy states as well.

For the amplification of coherent light the relation between spontaneous and stimulated emission occurrences is relevant as well. Photons created in spontaneous emission are not coherent, have a

random direction of travel, phase and polarization and can thus be regarded as background noise.[10] The relation between both processes is given in equation 13.

$$\frac{W_{m\to n}^{st.\ em.} N_m}{W_{m\to n}^{sp.\ em.} N_m} = \frac{\omega(\nu) B_{m\to n}}{A_{m\to n}} \overset{(9)}{=} \frac{1}{e^{\beta \cdot h\nu} - 1} = n(\nu) \tag{13}$$

Equation 13 is another condition in order to amplify coherent light, and states that stimulated emission has to dominate spontaneous emission.

2.2.2 Working principle of a laser

A simple model of a laser can be constructed by placing the system from chapter 2.1.2 between two mirrors with distance L and using an energy pump to considerably disturb the thermal equilibrium.[10] If a constant population inversion can be established, the medium is called active.[7] A visualization is given in figure 4. There are many methods for the pumping process, such as excitation through collision in some gas lasers, external electromagnetic radiation in solid-state lasers or injection of charge carriers in semiconductors.[10]

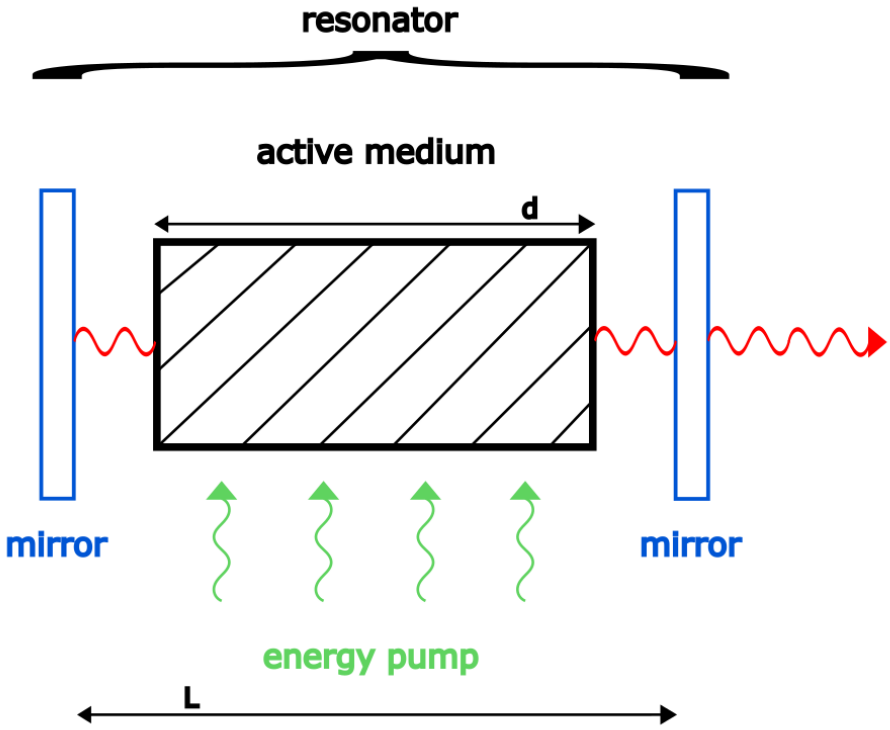

Figure 4: Visualization of a simplified laser model. The energy pump establishes an inversion population inside the medium. A standing wave will arise due to the resonance condition. The amplitude of the standing wave will increase due to stimulated emission and constructive interference. The laser light can be accessed via one semi transmitting mirror.[7]

If the distance between the two mirrors is selected with respect to the resonance condition (equation 14), standing waves with large amplitudes are generated, as waves in the resonator can interfere constructively.[9]

$$L = q \cdot \frac{\lambda}{2} = q \cdot \frac{c}{2 \cdot \nu} \tag{14}$$

Here, $q \in \mathbb{N}$, L denotes the distance of the two mirrors and λ denotes the wavelength of the light wave. Taking the resonance condition into account, stimulated emission can dominate spontaneous emission in the medium according to equation 13, since a high amplitude of light wave corresponds

to a high occupation number $n(\nu)$ of the radiation field inside the resonator.[9] The coherent laser light inside the resonator can be tapped by means of a semi-transparent mirror, see figure 4.[11]

The amplification of a light wave in the resonator can be derived via Beer's absorption law, which states that the intensity of the wave decreases exponentially with the travelling distance and a proportionality constant (equation 15).[7] Equation 9 shows that absorption and stimulated emission are determined by the same physics. This means that one can be treated as the inverse process of the other.

$$I(x,\nu) = I_{0,\nu} \cdot e^{-\alpha(\nu)\cdot x} \tag{15}$$

Here, x denotes the direction of travel and α is the coefficient of absorption given in equation 16

$$\alpha(\nu) = \left(N_m - \frac{g_m N_n}{g_n}\right) \cdot \sigma(\nu) \tag{16}$$

The absorption coefficient depends on the relation between the occupation numbers for the two energy states $|n\rangle$ and $|m\rangle$, the energy difference $E_m - E_n = h\nu$ and the absorption cross section $\sigma(\nu)$.[7] As previously mentioned the energy pump has established a constant population inversion $\Delta N_{inversion}^{population}$ inside the medium, i.e. equation 12, which can be rearranged to equation 17

$$\frac{g_m N_n}{g_n N_m} > 1 \Longrightarrow \Delta N_{inversion}^{population} = \frac{g_m N_n}{g_n} - N_m > 0 \tag{17}$$

Therefore, the term inside of the parenthesis in equation 16 is negative and the intensity is amplified while traveling.[7] Due to placing the active medium between the two mirrors a light wave can enter the active medium again after exiting it. The intensity of light after traveling a distance of $x = 2L$ becomes:[7]

$$I_{x,\nu} = I_{0,\nu} e^{-\alpha(\nu)\cdot 2d} \tag{18}$$

Thus, the gain G for the distance $x = 2L$, which can be called a revolution, becomes:[7]

$$G = \frac{I_{2d,\nu}}{I_{0,\nu}} = e^{-\alpha(\nu)\cdot 2d} \tag{19}$$

In a real application, losses, e.g. due to absorption in the mirrors and lateral leakage of light from the resonator, must also be considered. Taking into account losses $\delta(\nu)$ with the combination of equation 16 and the definition of $\Delta N_{inversion}^{population}$ from equation 17, the gain G' for one revolution becomes:[7]

$$G' = e^{-(2d\cdot\alpha(\nu)+\delta(\nu))} = e^{2d\cdot\Delta N_{inversion}^{population}\cdot\sigma(\nu)-\delta(\nu)} \tag{20}$$

From equation 20, a lower limit for the population inversion can be given as:[7]

$$\Delta N_{inversion}^{population} > \frac{\delta(\nu)}{2d\cdot\sigma(\nu)} \tag{21}$$

The first real laser was created in 1960 by Theodore Maiman and was based on a ruby crystal as medium.[10] The acronym "laser" denotes "Light Amplification by Stimulated Emission of Radiation".

2.2.3 Characteristics of laser light

The light from a general light source such as an incandescent lamp is non-directional and covers a broad spectrum of wavelengths, which is defined by Planck's law of radiation (see equation 7).[7]
In contrast, the light from a laser is highly directional, which means that it is emitted in a narrow beam. In addition, laser light is monochromatic, i.e. it consists of a single wavelength determined by the energy difference of the two involved energy states. Another important difference is that laser light is highly coherent, which means that the parameters like phase and polarization have a spatial and/or temporal correlation.[11]
In reality however, this is not always the case. Each laser differs in the degree of monochromaticity, coherence and also the quality of the beam shape.

2.3 Laser diodes

The laser effect in semiconductors was observed shortly after the realization of the first laser.[10] Laser diode systems are widely used today as they have several advantages, such as very small dimensions of $300\mu m \cdot 100\mu m \cdot 100\mu m$ and differential efficiencies of up to 50%.[10] In comparison, one of the most efficient gas lasers, e.g. CO_2, has a differential efficiency of $10 - 20\%$.[7]

2.3.1 Working principle of a laser diode

The simplest model of a laser diode is based on the concept of an LED, i.e. a light-emitting diode.[9] An LED is produced by combining two differently doped semiconductor materials.[12] An n-type semiconductor with an excess of electrons and a p-type semiconductor with an excess of holes, i.e. absence of electrons.[9] The doping of these materials is so high that the Fermi energy lies in the valence band of the p-type material and in the conduction band of the n-type material.[12] Figure 5 a.) and b.) show the pn-junction and the band model.

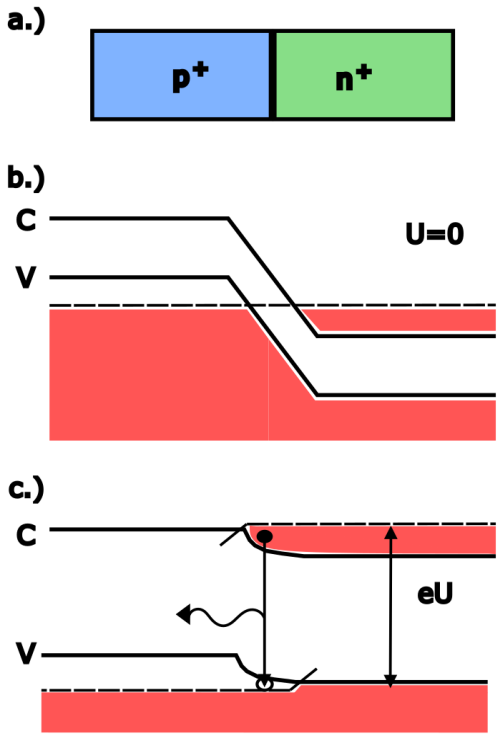

Figure 5: a: Contact of the highly doped semiconductors. b: Band model of the pn junction. c: Band model with current flow in forward direction. The occupied electron states are marked in red, the Fermi energy is represented in dashed lines and the valence and conductance bands are denoted with V and C.[9]

By applying a voltage to the LED, electrons and holes are attracted to the interface between the two materials, where they can recombine if the voltage is high enough to overcome the depletion zone.[12] During this recombination, photons are emitted with an energy corresponding to the band gap of the material, i.e. $E_\gamma = eU$.[12] However, these photons are emitted in random direction. The laser effect in an LED can be generated by inserting it in a resonator and applying high voltages.[9] In this way, a population inversion can be generated at the contact point. If the population inversion causes the stimulated emission to dominate the spontaneous emission, the LED starts to lase. An illustration can be found in figure 5 c.).[9] However, the electrical currents required for the population inversion are high, so that the LED can only be used as a laser in

pulsed mode.[9]

To generate coherent light in continuous-wave mode, a double heterostructure is used in which a lightly doped semiconductor is positioned between the p-type and n-type of the LED.[9] The band gap of the middle part must be smaller than the band gaps of the p-type and n-type semiconductor. An example is shown in figure 6 using the materials $Al_xGa_{1-x}As$ and $GaAs$. The band gap of $Al_xGa_{1-x}As$ can be varied between 1.42 eV ($GaAs$) and 2.17 eV ($AlAs$) due to different aluminum content ($0 \leq x \leq 1$).[9]

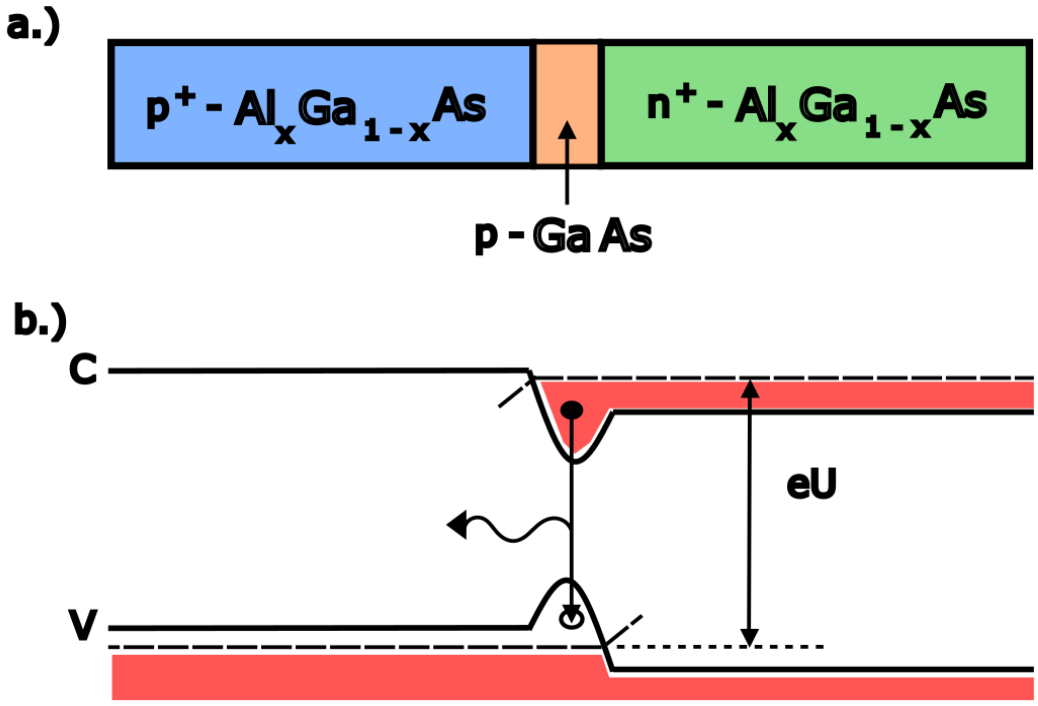

Figure 6: a: Heterostructure of the pn junction. b: Band model of the heterostructure with current flow in the forward direction to generate a population inversion in the middle layer. The occupied electron states are marked in red, the Fermi energy is represented in dashed lines and the valence and conductance bands are denoted with V and C.[9]

The use of $Al_xGa_{1-x}As$ has several advantages. First, the variable band gap allows the creation of energy barriers at the interfaces that trap electrons and holes in the center, i.e. in the active region.[13] This leads to a higher charge carrier density compared to the LED, which helps to achieve the necessary population inversion.[9] Second, the optical confinement ensures that the emitted photons are kept within the active layer, as $Al_xGa_{1-x}As$ has a higher refractive index than $GaAs$, leading to total reflections and thus making light amplification more efficient.[9]

By ensuring that the center region is thin and applying a voltage, electrons and holes can recombine efficiently in the active region.[9] This leads to a dense population inversion with more electrons in the excited state than in the ground state.[9] The recombination of these electrons and holes produces photons, which are confined in the active region. The photons induce more stimulated emission and can only leave the active medium at the sides of the active region, where there is no other material next to it.[14] Therefore, the structure acts as a resonator and amplifies light, leading to a coherent beam of light at one of the exits.[9] These types of diode lasers are known as edge-emitting diodes.[15]

2.3.2 Beam quality of a laser diode

The beam profile of a diode laser differs from that of other lasers in respect to beam shape. In a laser diode the light is bundled into a beam on one of the two sides of the active region. As the active region has a rectangular shape, the beam profile shortly after its exit has a similar shape, i.e. an elliptical shape. Due to the limited confinement, the laser beam is larger than the active region on the emitting side[15] This is shown in the figure 7.

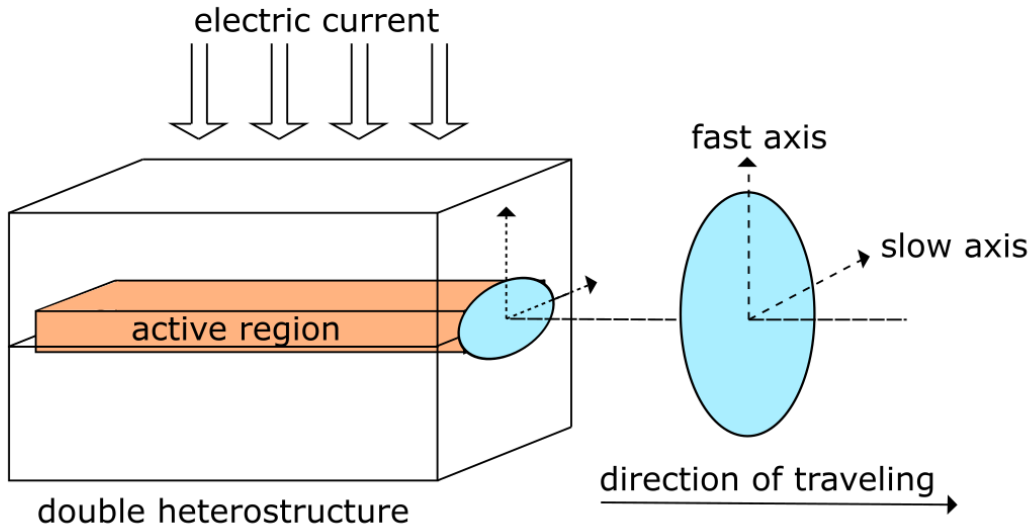

Figure 7: Beam shape of a general laser diode.[15]

As can be seen in the illustration in figure 7 the large semi-axis lies in the horizontal plane. However, this changes with increasing distance, as the light in the vertical plane has a different divergence than in the horizontal plane. The reason for the different divergences can be motivated with the help of a plane wave traveling through a single slit of size Δy, as shown in figure 8.

As shown in figure 8, light passes through the slit with an angular spread $\Delta\Theta$. The momentum of the light before the slit $p = (p_{x,0}, 0)$ was entirely along the x-direction. However, after the slit the momentum of the light beam p has now a component along the y-direction as well, i.e. $p = (\Delta p_x, \Delta p_y)$.The part along the y-direction Δp_y can be calculated due to energy conservation to:[14]

$$\Delta p_y = p \cdot sin(\Delta\Theta) \approx p \cdot \Delta\Theta \tag{22}$$

Here, the small angle approximation was used in the end. A lower limit for the spread Δp_y can be estimated with the help of Heisenberg's uncertainty principle. Which states that the product of the accuracy of position Δi and momentum Δp_i (i $\in \{x, y, z\}$) follows:[9]

$$\Delta i \cdot \Delta p_i \geq \frac{h}{4\pi} \tag{23}$$

Applying equation 22 to the principle of uncertainty leads to:[14]

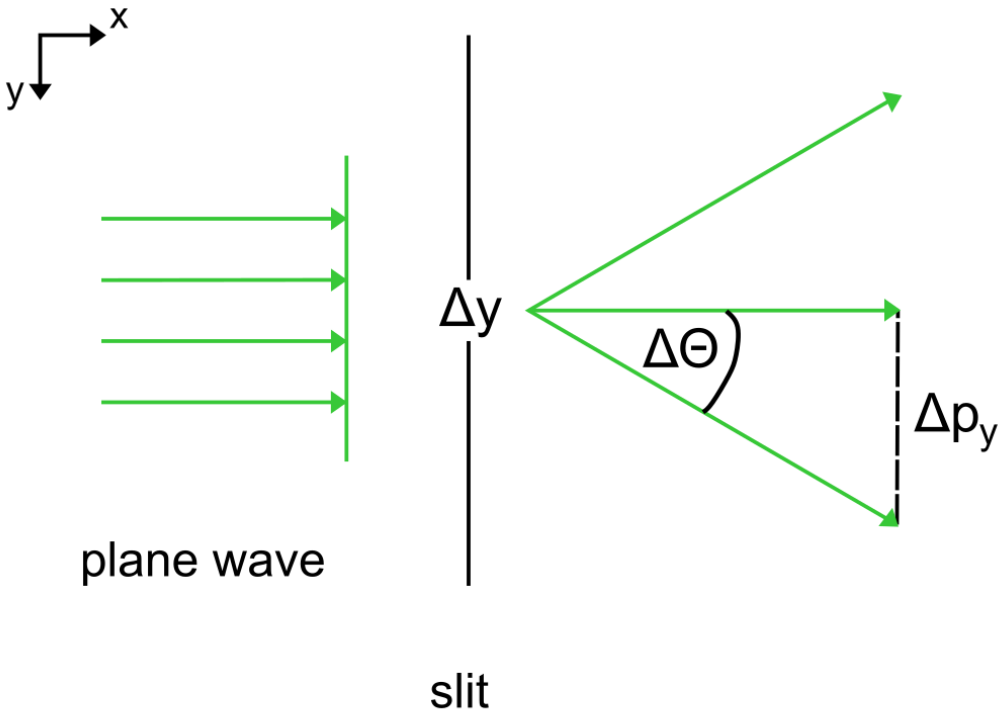

Figure 8: Plane wave traveling though a single slit.[14]

$$\Delta y \cdot \Delta p_y \geq \frac{h}{4\pi} \Longrightarrow \Delta y \cdot p \cdot \Delta\theta \geq \frac{h}{4\pi} \Longrightarrow \Delta\Theta \geq \frac{\lambda}{4\pi\Delta y} \tag{24}$$

In the last step the quantum-mechanical relationship between wavelength and momentum p was used, i.e. $p = \frac{h}{\lambda}$.[14] The spread $\Delta\Theta$ of the light beam relies on the ratio $\frac{\lambda}{\Delta y}$. Due to the rectangular shape of the active region, this ratio is not the same for the vertical and horizontal axis, thus leading to inherently different divergencies.[14]

In the end, the profile becomes an ellipse in the vertical plane, as the vertical divergence is greater. The axis with the greater divergence is known as the fast axis, while the other is known as the slow axis. This phenomenon is characteristic of a laser diode.[15]

3 Experimental setup & procedure

For the camera to monitor the position and shape of the 2 kW laser beam profile during CSR experiments, three requirements are necessary. First, the 2 kW laser is in the infrared (IR) range, thus the camera must not have an IR-filter. Most CMOS and CCD cameras posses a filter to block out IR-light, since it can lead to strange colors in daylight. Second, we need a camera that enables us to set a fixed gain and turn off the auto-gain. A constant gain will lead to consistent images, when the laser power is kept constant, since then pixel intensity is not varied leading to consistent intensities on the camera. A constant gain will also prevent possible problems with image capturing, if the 2 kW laser is operated in pulsed wavemode. For example, we already experienced that for certain repetition rates an automatic gain sets the gain too high in between pulses (due to a lack of another strong light source in the box), leading to overexposed (very bright or even white) images when the laser is captured by the camera on the power meter. The high intensities on the camera will then force the auto-gain to ramp down the gain value, leading to underexposed (dark or even black) images in between pulses. The last requirement regards the size of the camera. As indicated in the illustration of the photodetachment chamber (figure 2) in the motivation, there is very little space in the second laser box, where the camera could be placed to monitor the power meter. Therefore, the camera must be small. A rather inexpensive solution to this problem is the Raspberry Pi PiNoir Camera (Module V2) shown in figure 9a. This version of the raspberry pi cameras does not have an infrared filter and therefore is suited for the 808 nm of the laser. The camera is controlled via a Raspberry Pi (in our case the Raspberry Pi 4 (Model B) shown in figure 9b), that allows to control settings of the camera in Python on a rather deep level. More importantly we can control the gain, the shutter speed and the auto-white-balance (ABW).

(a) (b)

Figure 9: a: Raspberry Pi Noir Camera Module V2[16] b: Raspberry Pi 4 Model B[17]

For the method proposed in this thesis, the camera is connected to the Raspberry Pi, which hosts a website that streams the output of the camera in the format of Motion JPEG. The resolution of the stream is native full HD,[18] i.e. 1920 pixel horizontally and 1080 pixel vertically and has a framerate-per-second (fps) of 8. To be precise, we use RGB-JPEG because that enables us to switch between color and grayscale images. The format of a webstream is used, because the goal is to monitor the 2kW laser beam profile during experiments. With the Raspberry Pi we can control the camera settings and record images as frames of the webstream. For the experiment, the following camera settings have been chosen:

- auto-gain = off
- AWB = off
- ISO = 100
- shutterspeed = 25ms
- fps = 8

- camera.color_effects() = (128,128)

The last point is a command in the Python code that is executed by the Raspberry Pi and instructs the camera to capture grayscale images for this experiment. For more details, please refer to the Pi documentation.[18]

In the first part of the thesis, we want to find the working regime of the camera for the 2kW laser directed at the PM3K (setup from CSR). However, even with a low reflectivity of the PM3K, reflections of the 2 kW laser still could have enough power to completely over saturate the camera or even damage the hardware. For safety and usability reasons a test setup, consisting on a 15 mW laser diode at a wavelength of $\lambda = 650$ nm directed at the PM3K, is used. The power of the two lasers (2 kW and 15 mW) is separated by approximately 5 orders of magnitude. Therefore, the intensities seen by the camera should be comparable, if the filter which will be used in the CSR setup is 5 orders of optical density greater than the filter used for the working regime in the test setup. To determine the working regime of the camera in the test setup, the power curve of the 15 mW laser is measured with the power meter and the camera. The measurement with the power meter will be referred to as a power measurement and is straight forward. The laser is shot at the power meter at a certain distance of the laser and the power is measured for various voltages at the laser's power supply unit. At each measurement point, a photo of the laser profile on the power meter is also taken with the camera. The images measure the intensities on the camera, which are generated by the reflection of the laser profile on the power meter. This measurement will be referred to an intensity measurement. For the right working regime, the power curve from the power measurement and the intensity curve from the intensity measurement should have the same shape.

The PM3K is designed for the 2 kW laser and is therefore unsuitable for the 15 mW laser in the test setup with its power range of (0.1-3) kW.[5] In order to still be able to carry out the power measurement, we replace the PM3K with another power meter, the S120VC from Thorlabs, which has a power range of 50 nW to 50 mW.[19] A sketch of this experimental setup is shown in figure 10. It will be used to determine the necessary filters and the working regime of the camera for the 15 mW laser and the S120VC.

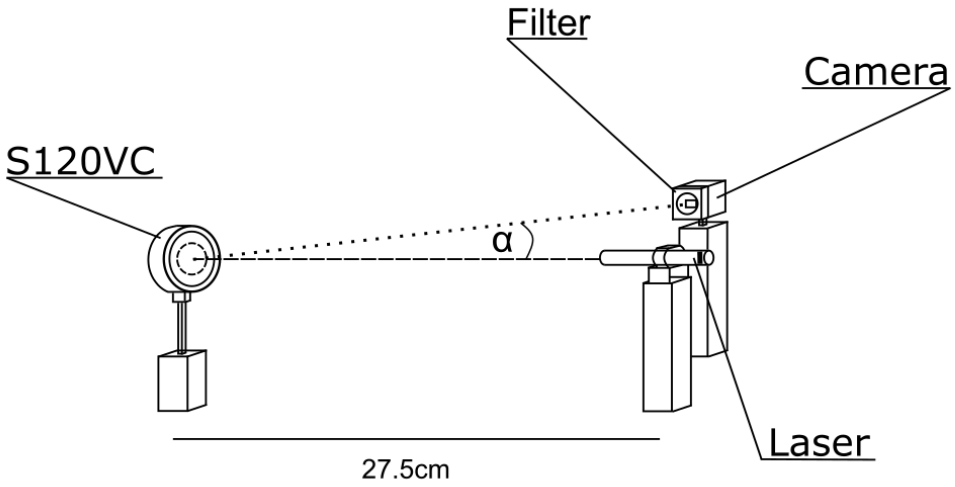

Figure 10: Experimental setup a: 15 mW laser directed at S120VC in a distance of 27.5 cm. The camera views the S120VC through a reflective optical density filter at an angle of $\alpha = 10.3°$ to the laser beam.

However, the S120VC has a different reflectivity than the PM3K. Therefore, the 15 mW laser is fired at the PM3K as soon as the working procedure for the S120VC has been established. With the new experimental setup (figure 11), intensity measurements are taken again and compared with the results (power and intensity measurement) of the working regime on the S120VC. This comparison will determine the necessary filter and the working regime for the 15 mW laser and the PM3K. Once the filter is known, we can give an estimate on the necessary filter for the CSR setup.

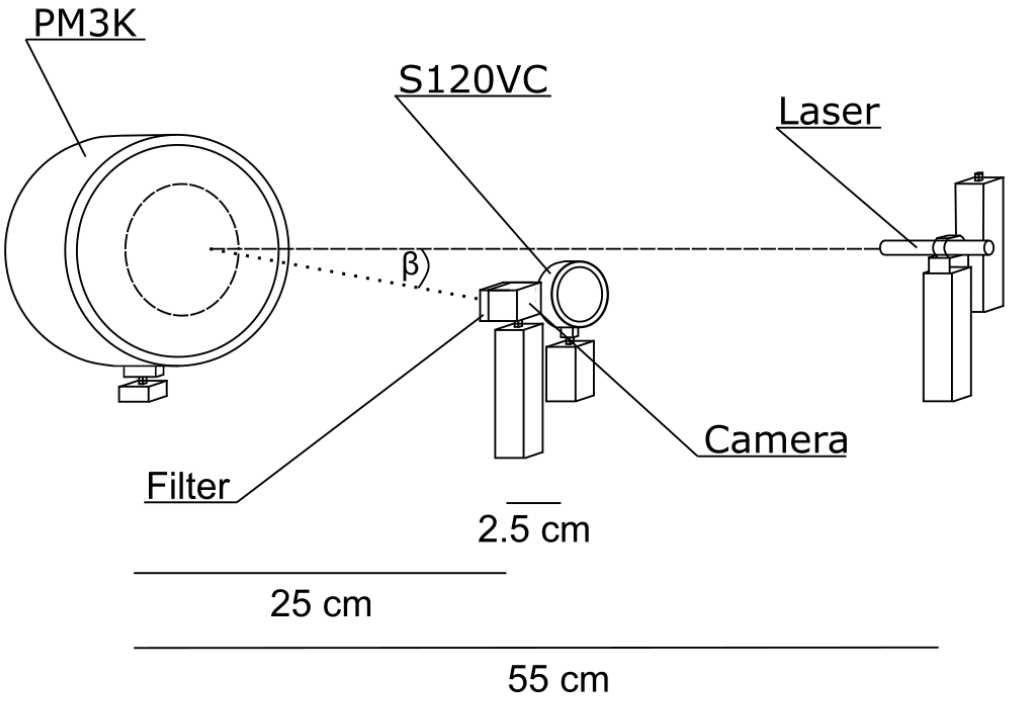

Figure 11: Experimental setup b: 15 mW laser diode directed at PM3K in a distance of 55 cm. The camera views the PM3K through a reflective optical density filters at an angle of $\beta = 11.31°$ to the laser beam.

Once the working regime for the camera is established, we can begin to analyze the beam shape. To do this, we first need to obtain reference values for the shape and position of the laser. For that, we will use an established method known as the knife-edge technique.[20] For this method, it is necessary to place a plate in front of the laser that can be moved through the laser beam in a line perpendicular to it. The plate can therefore block a certain part of the beam for each position. Behind the plate is a measuring device placed that measures the power of the beam for each position of the plate. If the laser is kept at constant power during this measurement, the power value for each plate position provides information on how much laser intensity has been "cut off" (blocked) by the plate. Thus the data leads to information about shape and position of the laser profile on the measuring device projected along the direction of propagation of the plate. The construction we used in our experiment is placed 17.5 cm away from the laser and consists of a black anodised plate mounted on a platform. The plate can be moved into the beam in 10μm steps using a precision screw. For the power measuring device, we used the S120VC at a distance of 27.5 cm from the laser. For this part of the thesis we used a 10 mW laser diode operating at a wavelength of $\lambda = 650$ nm in continuous wavemode. The camera views the S120VC at an angle $\alpha = 10.3°$ to the laser beam. Furthermore, we placed a reflective neutral density filter OD 2 in front of the camera. The construction we use is only able to move in a horizontal line. To also obtain information about the vertical projection of the laser profile, we must rotate the 10 mW laser by 90° by hand and repeat the measurement process. The experimental setup is shown in Figure 12.

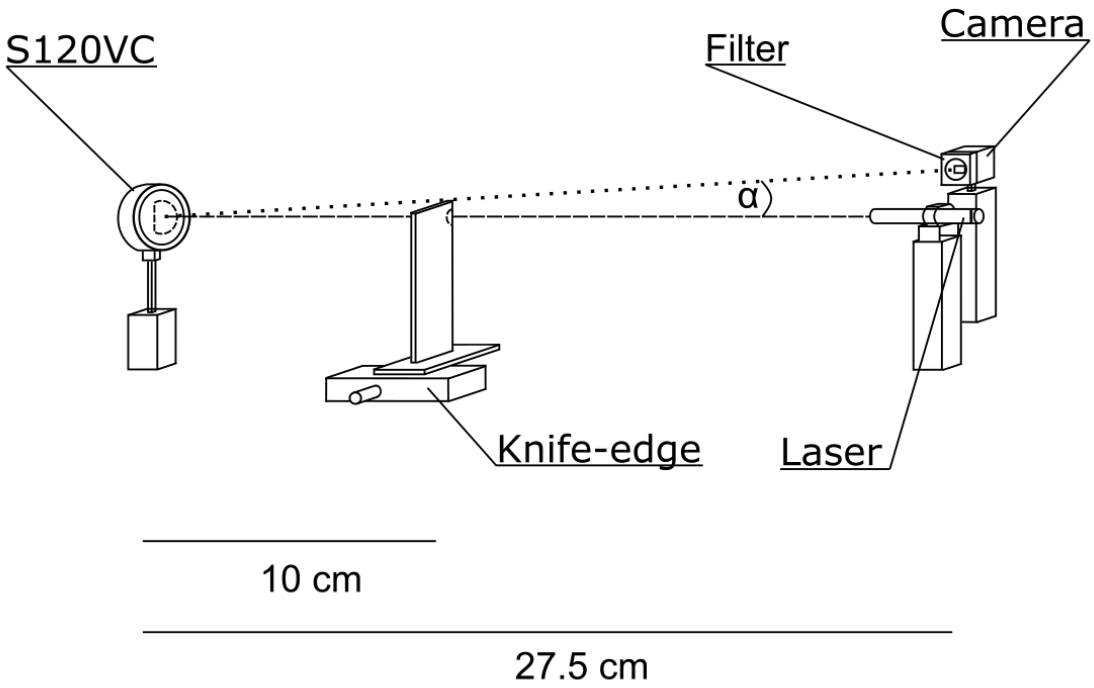

Figure 12: Experimental setup c: 10 mW laser directed at S120VC in a distance of 27.5 cm. A black anodized plate mounted on a platform is placed 17.5 cm away from the laser. The plate can be moved into the beam in 10μm steps using a precision screw. The camera views the S120VC through a reflective filter OD 2 at an angle of $\alpha = 10.3°$ to the laser beam.

The camera results for shape and position are obtained from images (where the plate does not block the laser beam) of the 10 mW laser on the S120VC. In general, information of any projection of the laser profile can be extracted from one image. To compare the results of the camera method with the reference method, we project the laser profile from the camera results onto the same axes (horizontal and vertical). However, since the 10 mW laser has to be rotated for the reference method, we take two images of the laser profile (one for each knife-edge measurement) to minimize errors due to not exactly turning the 10 mW laser diode by 90 degrees. This will simultaneously avoid an error due to changing the focus of the laser in between the knife-edge measurements, since the focus of the laser diodes used in the experiments are changed by rotating the top of the laser diode. This experiment is divided into two runs, with each run consisting of a knife-edge measurement and a camera measurement. The results will then lead to a comparison of the beam profile derived with both methods. A top view of all experimental setups used in this work can be found in the appendix A in figure 34.

4 Evaluation

The evaluation of this work can be divided into two different parts. In the first part, we will determine the working regime of the camera for the 2 kW laser and the PM3K. In the second part, we will compare the laser beam profile measured with the knife-edge technique (reference measurement) to the results of the camera measurement.

4.1 Working regime of the camera for the 2 kW laser and the PM3K

To determine the working regime of the camera for the 2 kW laser and the PM3K, we start with the working regime for the 15 mW laser and the S120VC.

4.1.1 Working regime of camera for a 15 mW laser and the S120VC

For the determination of the working regime of the camera for the 15 mW laser and the S120VC, we used the experimental setup shown in figure 10. For the power measurement, we measured the power of the 15 mW laser on the S120VC for voltages in the range of (1.3-5) V in steps of 0.1 V and took a measurement at 0 V for background correction. For the power measurement, we started at 1.3 V, as the laser on the S120VC was already faintly visible to the naked eye at this value but the power values on the S120VC did not change. For the intensity measurement, we captured an image with the camera of the laser beam profile on the S120VC for each voltage value. The camera results will be discussed after the power results. The result for the power measurement is given in figure 13.

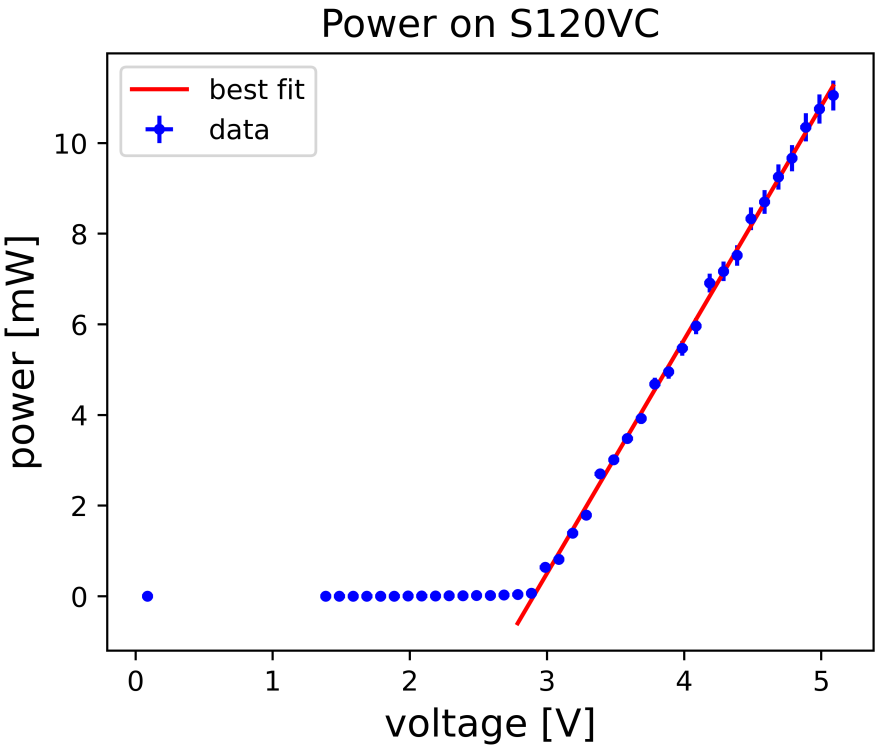

Figure 13: Power of 15 mW laser on the S120VC.

The results for the power measurement of the laser indicate two regions (zero and linear). The second part starting around 3 V shows a linear relationship that can be described by equation 34 between power on the S120VC and supplied voltage of the laser diode.

$$f(x, a, b) = a \cdot x + b \tag{25}$$

The parameters of the fit are given in table 1.

Table 1: Parameters of the fit for power measurement of the 15 mW laser on the S120VC (figure 13)

a	(5.16 ± 0.05) $\frac{mW}{V}$
b	(-14.97 ± 0.19) mW
x_{off}	(2.90 ± 0.04) V

The x-offset (x_{off}) and its uncertainty ($\sigma_{x_{off}}$) have been calculated with equation 26 and gaussian error propagation (equation 27).

$$x_{off} = -\frac{b}{a} \tag{26}$$

.

$$\sigma_{x_{off}} = \sqrt{\left(\frac{\sigma_b}{a}\right)^2 + \left(\frac{b \cdot \sigma_a}{a^2}\right)^2} \tag{27}$$

The zero part in the power measurement between 1.3 V and 3 V, indicates a non-linear part ranging from 2 V to around 3 V. This part is only visible by zooming to that region and shown in figure 14. This is probably the regime where the stimulated emission is not yet stronger than spontaneous emission (see equation 13 in chapter 2.2) and therefore the laser diode is not lasing yet.

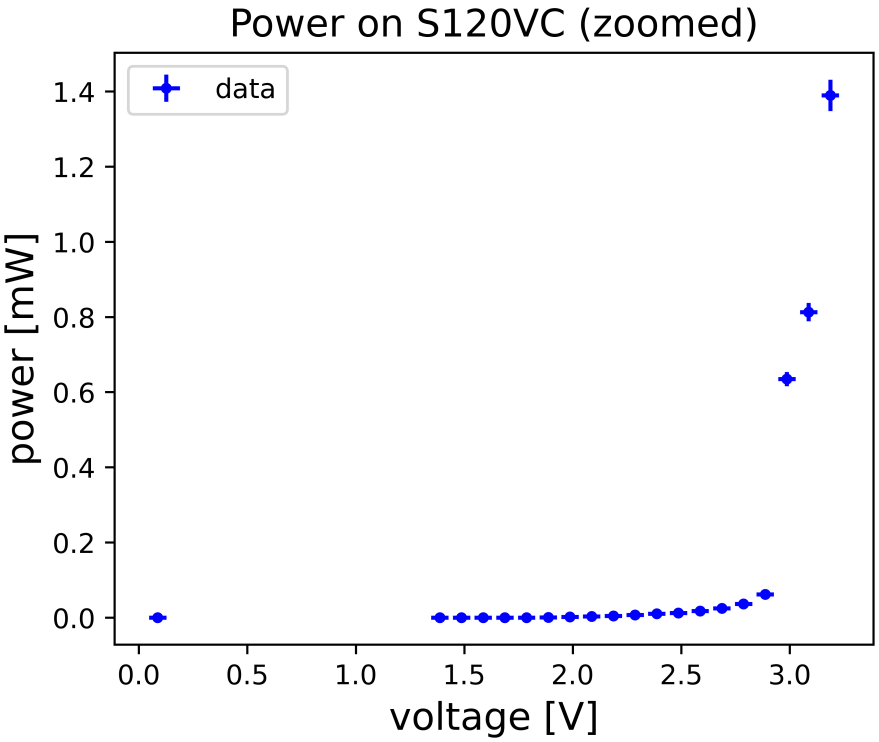

Figure 14: Power of 15 mW laser on the S120VC from figure 13 (zoomed).

We estimated the uncertainty of the supplied voltages v with the help of two additional measurements. For these measurements, we set the power supply unit to values ranging from 1.3 V to 5 V and measured the applied voltage separately with a multimeter (UT131B Multimeter from

UNI-T) in steps of 0.1 V, while the laser was connected and running.[21] The multimeter has an uncertainty of ±0.7% for voltages under 0.2 V and ±0.5% for voltages under 20 V.[21] The results are shown in the figure 35 in the appendix B.1. The uncertainty for the voltage values is $\Delta v = 0.04$V (the determination is given in the appendix B.1 as well). The powermeter has an uncertainty of 3% in the wavelength range of 440-980 nm according to the manufacturer.[19]

After we have discussed the results for the power measurement of the 15 mW laser on S120VC, we can start evaluating the results of the intensity measurement with the camera. The images are taken out of a videostream on a website hosted by the raspberry pi. The format of the videostream is Motion JPEG, hence each frame in the video stream is a JPEG image and the images are saved as frames of the stream. The resolution of the images is native Full HD, i.e. 1920 pixels horizontally and 1080 pixels vertically, and they are saved in RGB-JPEG format. This format uses the RGB colour space with three components, each of which has 8 bits. The number of possible combinations in one color channel is thus $2^8 = 256$. Therefore, the i-th pixel in a JPEG image has three values $(p_{i,r}, p_{i,g}, p_{i,b})$ ranging between (0,0,0) and (255,255,255).[18] However, we set the camera to capture grayscales during the experiment, therefore, the raspberry pi converts the output of the camera from grayscale into RGB-JPEG. During this conversion the i-th pixel $p_i^{grayscale} = (x)$ $(0 \leq x \leq 255)$ from the grayscale image becomes $p_i^{rgb-jpeg} = (x, x, x)$ in the RGB-JPEG format. During the evaluation we found out that there is a conversion error on average of under 1% between the three components of each pixel. We average the channels of each pixel to minimize conversion errors with equation 28.

$$\bar{p}_i = \sum_{j=r,g,b} p_{i,j} \tag{28}$$

Due to the reflective filter in front of the camera during the measurement we see reflections besides the actual laser profile in the images. Figure 15a shows a typical image taken by the camera during the experiment. To eliminate reflections, we cut out the laser profile with an elliptical shape and place it in a completely black image of the same size. Figure 15b shows a zoomed version of the "cut" (cropped) image.

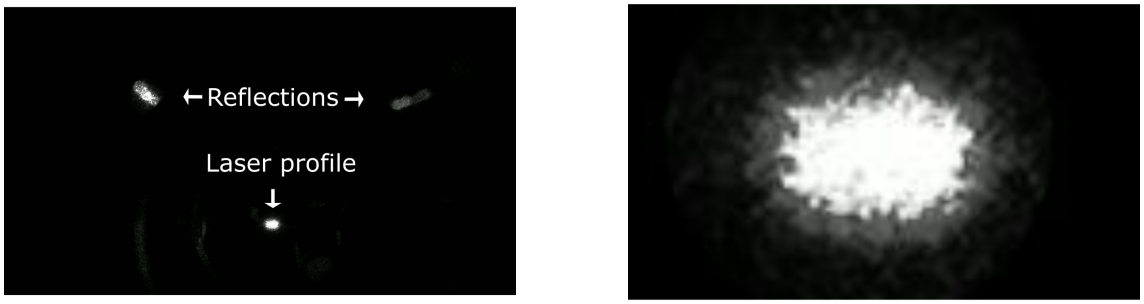

(a) (b)

Figure 15: Elimination process of reflections seen in the captured image with the camera for the 15 mW laser on the S120VC at 5 V. a: captured image. b: image (zoomed to profile) after elimination procedure

We believe that the total intensity seen by the camera correlates roughly linearly to the power of the 15 mW laser on the S120VC. To obtain one value of each image representing the intensity seen by the camera, we sum up the values of all pixels. This minimizes stochastic errors in comparison to taking a few or just one pixel for each image. The sum over all pixels will be referred to as total-intensity I_{xV} $(1.3V \leq x \leq 5V)$ and is mathematically described by equation 29.

$$I_{xV} = \sum_{i=1}^{1920 \cdot 1080} \bar{p}_i \tag{29}$$

All intensities have been corrected by the intensity I_{0V} from the image of the background measurement at 0 V. Figure 16 shows the result of the intensity measurement.

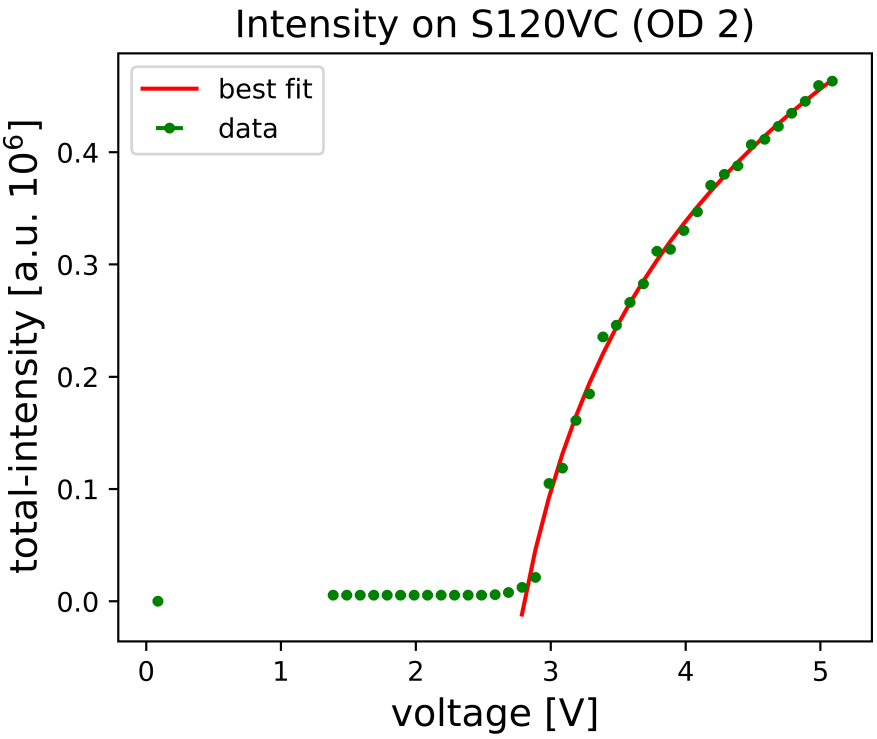

Figure 16: Intensity seen by the camera (OD 2 filter) of the 15 mW laser on the S120VC.

The camera results show two parts of the spectrum, a zero part and a non-linear part. The first part can again be explained by the onset of the laser process. The second part however, is different to the results of the power measurement (figure 13). The results indicate a non-linear relationship between observed total-intensity with the camera and supplied voltage of the laser. To be more specific, we were able to fit a logarithmic function to that part of the results, according to equation 30.

$$f(x, a, b, c) = a \cdot ln(x - b) + c \tag{30}$$

Fitting equation 30 resulted in the following parameters.

Table 2: Parameters of the fit for the intensity measurement with the camera (through a OD 2 filter) of the 15 mW laser on the the S120VC.

a	$(0.244 \pm 0.015) \times 10^6 \frac{\text{a.u.}}{\text{V}}$
b	(2.42 ± 0.08) V
c	$(0.207 \pm 0.020) \times 10^6$ a.u.
x_{off}	(2.81 ± 0.09) V

The x-offset (x_{off}) has been calculated via 31 and the fit parameters a, b and c.

$$x_{off} = exp(-\frac{c}{a}) + b \tag{31}$$

The uncertainty $\sigma_{x_{off}}$ was calculated with gaussian error propagation (equation 32).

$$\sigma_{x_{off}} = \sqrt{\left(\frac{\sigma_c}{a} exp\left(-\frac{c}{a}\right)\right)^2 + \sigma_b^2 + \left(\frac{c \cdot \sigma_a}{a^2} exp\left(-\frac{c}{a}\right)\right)^2} \tag{32}$$

Now that we have discussed both results (power and intensity), we can address the question of the working range of the camera for the 15 mW laser and the S120VC. Contrary to our assumption, that the intensity observed with the camera correlates linearly with the power on the S120VC, we have seen in the results that the camera shows a non-linear response in the area, where the power measurement gives a linear response. We believe that this is an effect due to saturation of pixels and therefore not capturing images in the working regime of the camera.

To test this hypothesis, we choose 5 equidistant pixel (which lie in one line) with a separation of 10 pixel inside the brightest part of the laser profile and plotted their value with respect to the supplied voltage of the 15 mW laser. We call those pixel "bright" pixel and a visualization is given in figure 17. In the visualization a grid is used to represent individual pixel as squares and the green filled squares represent "bright" pixel. Due to overview reasons the grid is not to scale, which lead us to only mark 3 "bright" pixel with a distance of 5 pixels (squares) in the illustration.

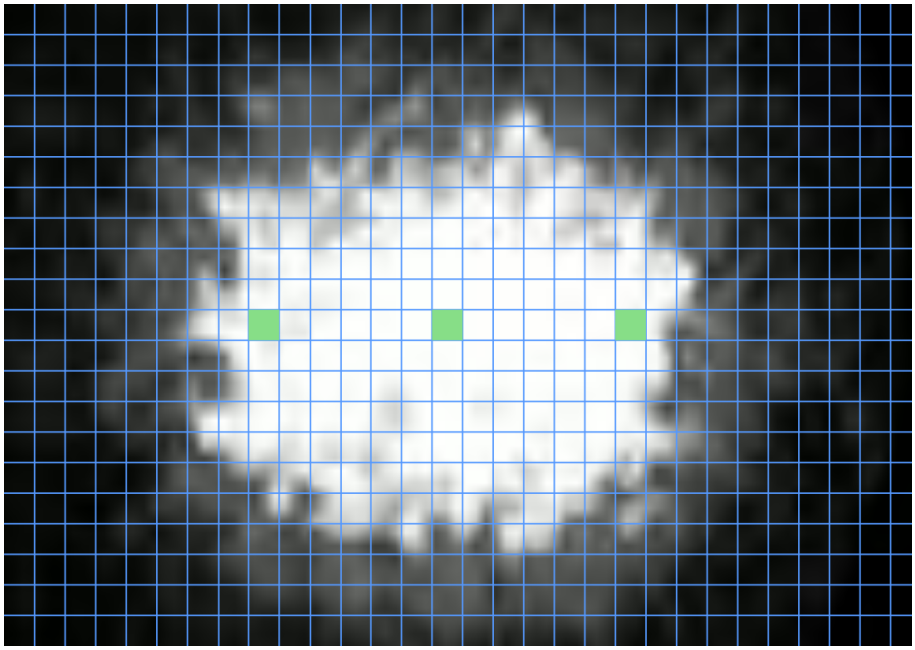

Figure 17: Visualization of "bright" pixel (green squares). The grid is not to scale and each square represents a pixel.

Figure 18 shows the results and the mean of the 5 "bright" pixels.

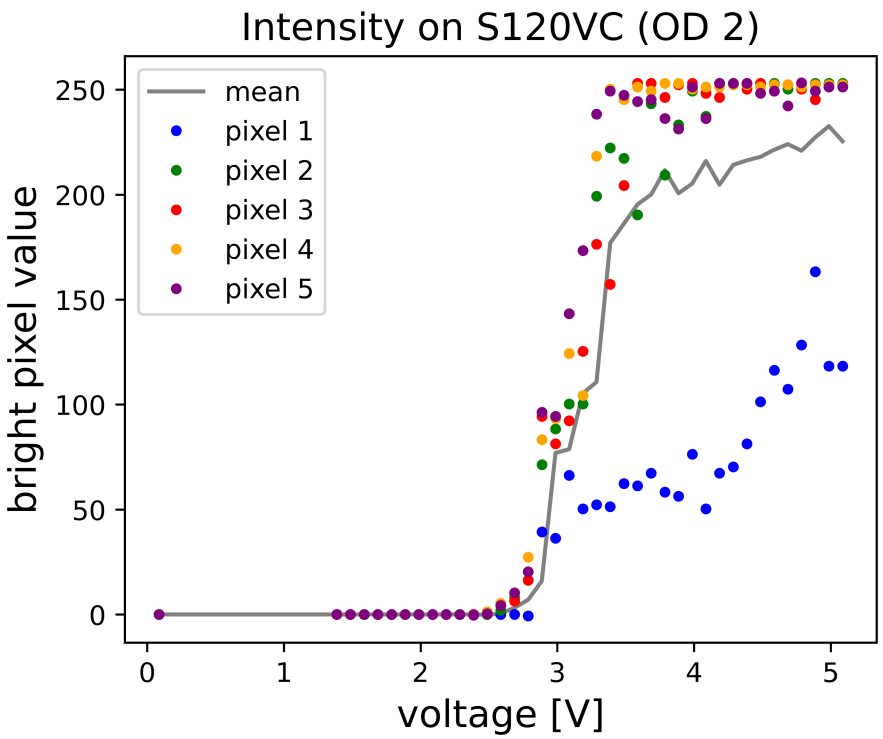

Figure 18: "Bright" pixel intensities from camera results (figure 16) for 15 mW laser on the S120VC.

We can see that 4 out of 5 "bright" pixel went into saturation during the intensity measurement (figure 16), which could explain the non-linear relationship between the intensities observed with the camera and the supply voltages of the 15 mW laser on the S120VC.

To avoid saturation effects of individual pixels, and test if the saturation is the reason for the non linear behaviour of the camera, we ran the experiment again. This time we increased the profile of the 15 mW laser on the S120VC to minimise the intensity of individual pixels. We defocused the 15 mW laser, resulting in an 23% larger beam profile ("lbp" for short) on the S120VC compared to the first run. The result of the power measurement on the S120VC is analogue and can be found int the appendix B.2 in figure 36. The result for the intensity measurement with the camera is given in figure 19.

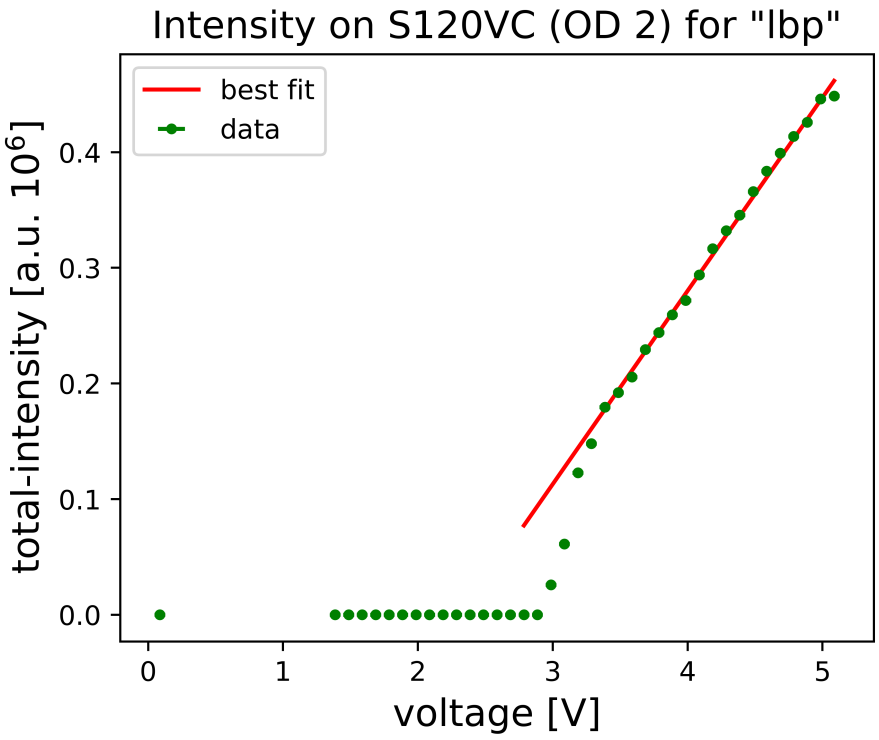

Figure 19: Intensity seen by the camera (OD 2 filter) of the 15 mW laser with 23% larger beam profile ("lbp") on the S120VC.

The camera results show three different areas in the spectrum (zero, non-linear and linear). The zero part presumably comes back to the weak laser light for voltages $\leq$ 2-3 V (compare to the power measurement in figure 14). We assume that the non linear part around 3 V could be due to threshold effects of the camera. The last part shows a linear relationship between the intensity seen by the camera (through a OD 2 filter) and the supplied voltages of the 15 mW laser. We made a fit with the following equation to the last part of the spectrum:

$$f(x, a, b) = a \cdot x + b \tag{33}$$

The resulting parameters are given in table 3 below.

Table 3: Parameters of the fit for intensity measurement of the 15 mW laser on the S120VC (figure 19)

a	$(0.1672 \pm 0.0022) \times 10^6 \frac{\text{a.u.}}{\text{V}}$
b	$(-0.389 \pm 0.010) \times 10^6$ a.u.
x_{off}	(2.33±0.06)V

The x-offset (x_{off}) and its uncertainty ($\sigma_{x_{off}}$) have been calculated with equation 26 and gaussian error propagation (equation 27).

In order to verify, that the increase by 23% of the beam profile on the S120VC indeed avoided saturation of individual pixel we give the value of "bright" pixel (chosen after the method shown in figure 17) for this intensity measurement as well.

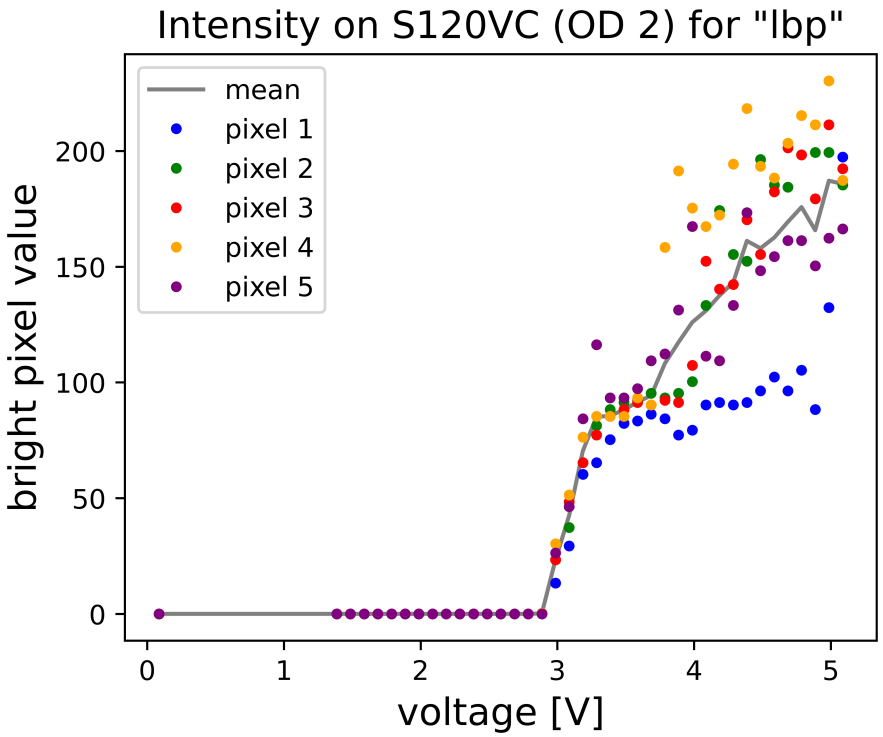

Figure 20: "Bright" pixel from intensity measurement with camera (figure 19) for 15 mW laser with a 23% larger beam profile ("lbp") on the S120VC.

Figure 20 shows that enlarging the beam profile on the S120VC decreased the intensity perceived by individual pixels and avoided saturation effects. Furthermore, the results indicate three regions, as observed in the results for the total intensity, i.e. a zero part until 2-3 V, a non-linear part starting around 3 V and and a linear part after 3.4 V (compare to figure 19). This also shows, that the logarithmic behavior that we have seen before (figure 16) was due to saturation of individual pixels and operation outside the linear regime. Even though the laser profile of the 15 mW laser did not move on the S120VC during the experiments, we can see fluctuations between the values of individual "bright" pixels, which probably are of stochastic nature.

We are now able to give a statement on the working regime of the camera for the 15 mW laser and the S120VC. The total-intensity observed by the camera should be as high as possible (while avoiding saturation) to avoid the non-linear regime of the spectrum (figure 19). Nevertheless, the intensity of individual pixel should be controlled by appropriate filters of optical density or by enlargement of the laser beam profile. As a limit we give an intensity value of 230 per pixel, since it was the highest value reached by "bright" pixel 4 (figure 20) in the run with an 23% larger beam profile ("lbp"). Now that we know the working regime of the camera for the setup used in this measurement (15 mW laser and S120VC), we can try to figure out the working regime for the 15 mW and the PM3K.

4.1.2 Working regime of the camera for the 15 mW/2 kW laser and the PM3K

In the last chapter we determined the working regime for the 15 mW laser and the S120VC. In this chapter, we would like to use that information to obtain the working regime of the 15 mW laser impinging on the PM3K, and give an estimation for the OD-Filter that should be used with the 2kW laser. To do this, we need the experimental setup shown in figure 11, which involves the camera monitoring the PM3K and the 15 mW laser directed at the PM3K. We did this measurement twice, first with a filter of OD 0 (i.e. no filter) placed in front of the camera and second with a filter of OD 0.3. The filter have lower optical density than the filters that were used with the S120VC, since the PM3K has a lower reflectivity. To further simulate the conditions of the CSR setup (2 kW laser and PM3K), we will adjust our laser beam profile on the PM3K to be comparable in size. During early test-runs with the 2kW laser, a color image was taken of the laser beam profile on the PM3K, which is shown in figure 21.

(a) (b)

Figure 21: 2 kW laser beam profile on the PM3K in the photodetachment chamber of the CSR. Laser operated in continuous wavemode and 100 ms were selected as exposure time for the camera. a: View of the PM3K with 2 kW laser off and laser box 2 opened. b: View of the PM3K with 2 kW laser turned on and laser box 2 closed.

Figure 21a shows the view of the camera inside the photodetachment chamber, while the 2 kW laser was turned off and the second laser box opened. This image is helpful to better show where the PM3K is in figure 21b. This image shows the 2 kW laser beam profile during laser operation. It should be mentioned again, that the 2 kW laser operates in the near infrared regime and the color seen in figure 21b does not correspond to its wavelength ($\lambda = 808$ nm), but is made visible for the naked eye by the camera (Raspberry Pi Camera Module 2 NoIR).[22] Figure 22 shows the 15 mW laser beam profile on the PM3K in our experiment.

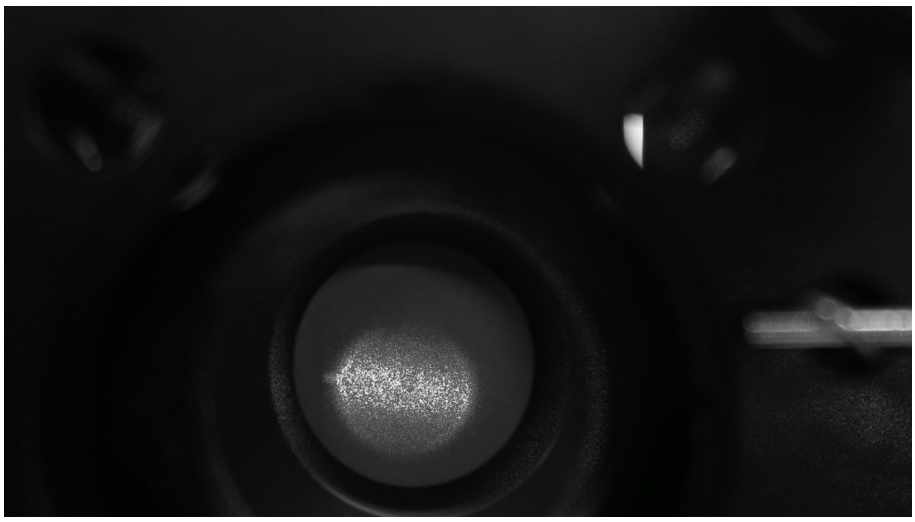

Figure 22: 15 mW laser beam profile on the PM3K in our experiment (experimental setup shown in figure 10) for operation in continuous wavemode and selected exposure time of 25 ms for the camera. The camera is programmed to take grayscales, therefore the 15 mW laser appears grey even though it operates in the visible spectrum.

We will now conduct two intensity measurements analog to the intensity measurements for the S120VC. The results for the intensity measurements with the camera are given in figure 23.

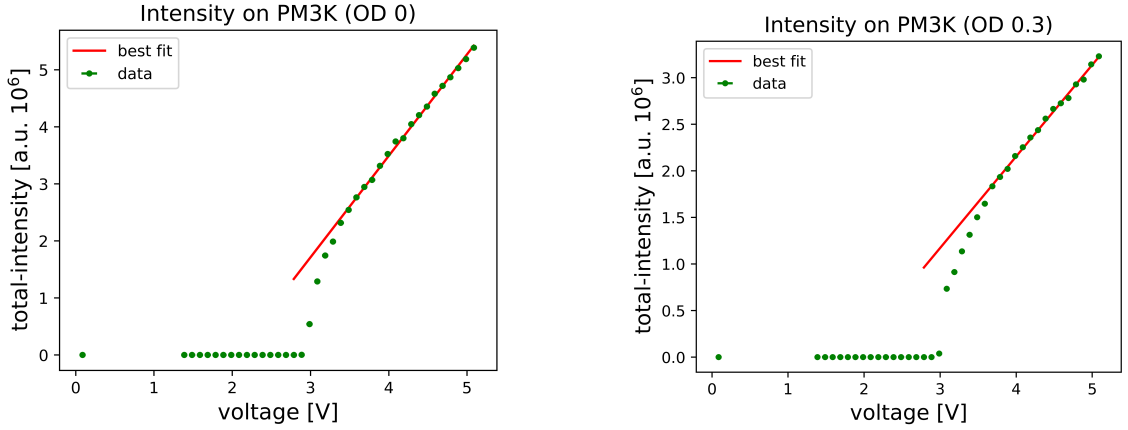

(a) (b)

Figure 23: a: Intensity seen by the camera (no filter) of the 15 mW laser on the PM3K. b: Intensity seen by the camera (OD 0.3 filter) of the 15 mW laser on the PM3K.

The results indicate the same three parts (zero, non-linear and linear) as seen in the intensity measurement of the 15 mW laser with a 23% larger laser beam profile ("lbp") on the S120VC (figure 19). This means that for higher intensities, the intensity measured with the camera correlates linearly to the power output of the 15 mW laser on the PM3K. We fitted again a linear function to the last part of the spectrum with:

$$f(x, a, b) = a \cdot x + b \tag{34}$$

The parameter of both fits are given in the table below:

Table 4: Parameters of the fit for intensity measurement of the 15 mW laser on the PM3K (figure 23a and 23b)

	OD 0	OD 0.3
a	(1.779 ± 0.021) $\times 10^6$ $[\frac{a.u.}{V}]$	(0.983 ± 0.015) $\times 10^6$ $[\frac{a.u.}{V}]$
b	(-3.63 ± 0.09) 10^6 [a.u.]	(-1.78 ± 0.07) 10^6[a.u.]
x_{off}	(2.04 ± 0.06) [V]	(1.81 ± 0.07) [V]

The x-offset x_{off} and its uncertainty $\sigma_{x_{off}}$ have been calculated like before with equation 26 and 27. In order to give an estimation on what reflective neutral density filter should be placed before the camera in the CSR setup, we will have a look at "bright" pixel of these two intensity measurements. The "bright" pixel have been chosen as before (illustrated in figure 17) and the results are given in figure 24.

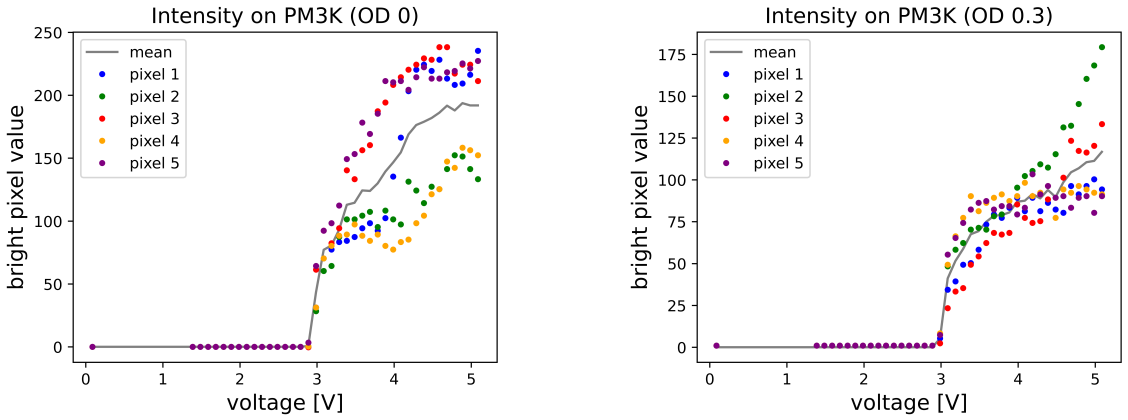

(a) (b)

Figure 24: a: "Bright" pixel from intensity measurement with camera (figure 23a) for 15 mW laser on the PM3K. b:"Bright" pixel from intensity measurement with camera (figure 23b) for 15 mW laser on the PM3K.

The results indicate that even though the total intensity in both measurements (figure 23) showed a linear regime, individual "bright" pixel (pixel 1, 3 and 5) start approaching the saturation value of 255 in the measurement with no filter in front of the camera (figure 24a). On the other hand, figure 24b shows that no "bright" pixel started saturating for the measurement with a reflective neutral density filters OD 0.3 for very high intensities. Based on those results we estimate that a reflective filter of OD 5.3 should be used with the 2 kW laser at the CSR.

4.2 Shape and position of a 10 mW laser profile on the S120VC

In this part of the thesis we will determine the shape and position of a 10 mW laser beam using the knife-edge measurement as a reference and compare it to the camera.

4.2.1 Reference measurement

For the reference measurement we used the experimental setup involving the knife-edge construction, the 10 mW laser directed at the S120VC and the camera monitoring the S120VC as shown in figure 12. We kept the power of the 10 mW laser constant on the S120VC, due to a constant supply of (4.50±0.05) V. For the first knife-edge measurement, we moved the plate over distance of $x_1 = 680\mu$m in a step size of 10μm and measured the power on the S120VC for each step. The result is given in figure 25a. After the first measurement, we rotated the 10 mW laser diode by 90° by hand and repeated the measurement. This time we moved the plate over a distance of $x_2 = 590\mu$m. The result is given in figure 25b.

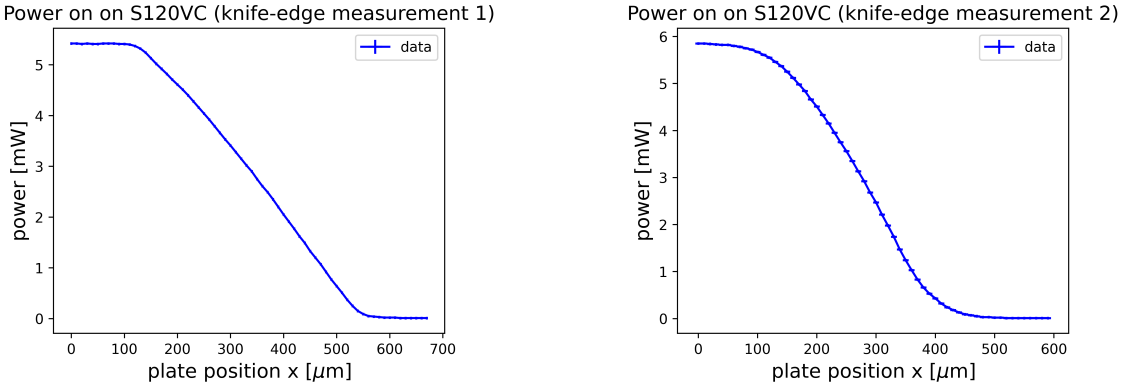

(a) (b)

Figure 25: Power of 10 mW laser on S120VC for the knife-edge measurement. The plate was moved over a distance of a: $x_{slow} = 680\mu$m in the first run. b: $x_{fast} = 590\mu$m in the second run.

The uncertainty in position σ_x for each measuring point is estimated via half a turn, i.e. $\sigma_x = 5\mu$m. The uncertainty σ_p for the measured power p on the S120VC for each step is given due to the linearity error from the manufacturer, i.e. 0.5% from the maximum power value of each measurement.[19]

The beam shape of the 10 mW laser can be extracted out of the knife-edge results according to the following logic. Let's assume a one dimensional beam profile $F(x)$ with amplitude A, center μ and standard deviation σ according to a gaussian intensity distribution.

$$F(x) = A \cdot \exp\left(-\frac{(x-\mu)^2}{2\sigma^2}\right) \tag{35}$$

In the general knife-edge approach, the plate is not consecutively moved into the laser beam, but out of it. That means, that the plate resides at a position x_{block} at which the laser beam is entirely blocked and is then consecutively moved out. This means that for every step, a tiny slice is added to the the laser intensity on the measuring device behind the plate. Therefore, the power values $p(x)$ are accumulated until the plate is entirely moved out off the laser beam and the total laser intensity is measured on the device.[20] This procedure can be explained mathematically via:

$$p(x) = \int_{-\infty}^{x_{block}} F(x) = -\int_{0}^{x_{end}} F(x) \tag{36}$$

In the last step, we took into account that we moved the plate from a position, where it did not block the laser beam ($x = 0$) to a position, where it was completely blocked (x_{end}), which leads to a change in the integration limits and a minus sign.[20] Taking the negative derivative of our power data $p(x)$ from the knife-edge measurement should lead to the original beam profile $F(x)$.

$$F(x) = -\frac{dp(x)}{dx} \tag{37}$$

We calculated the derivative numerically for each measurement point p_i with the help of the neighboring measurement points p_{i-1} and p_{i+1}:

$$p'(x_i) \approx \frac{p(x_{i+1}) - p(x_{i-1})}{x_{i+1} - x_{i-1}} \tag{38}$$

Here, $p'(x_i)$ denotes the derivative for the i-th power value from the knife-edge measurements (x_{i+1}, p_{i+1}) and (x_{i-1}, p_{i-1}), which denote the two measurement points next to it. For the first and last power value, i.e. p_0 and p_{end} the derivative was calculated similar to equation 38 but with the value itself as one of the two neighbors. Equation 39 shows this for the first value.

$$p'_0(x_0) \approx \frac{p(x_1) - p(x_0)}{x_1 - x_0} \tag{39}$$

The results of the laser profiles from the knife-edge measurements are given in figure 26.

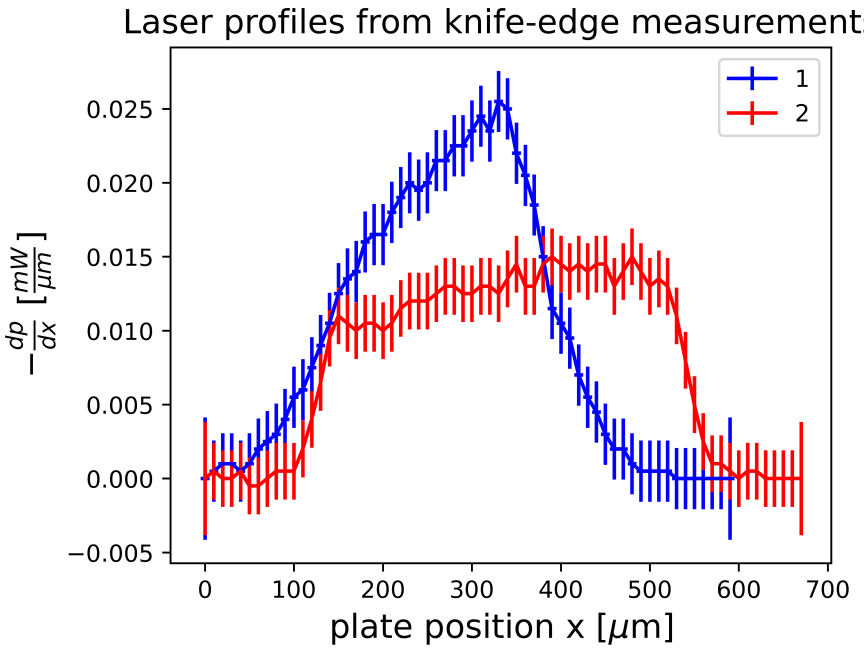

Figure 26: Laser profiles from knife-edge measurements (figure 25). The 10 mW laser diode was turned by 90° between measurement 1 and 2.

The errors have been calculated with Gaussian error propagation. To simplify the math let us make the following substitutions in equation 38 of the numerical derivative for each power value p_i:

- $p'(x_i) = f$
- $p(x_{i+1}) = a$
- $p(x_{i-1}) = b$

The uncertainty we now calculate is for:

$$f \approx \frac{a-b}{x_{i+1}-x_{i-1}} \tag{40}$$

The variables a, b, x_{i+1} and x_{i-1} have uncertainties of σ_a, σ_b, $\sigma_{x_{i+1}}$ and $\sigma_{x_{i-1}}$. Gaussian error propagation for equation 40 leads to:

$$\sigma_f = \sqrt{(\frac{\partial f}{\partial a}\sigma_a)^2 + (\frac{\partial f}{\partial b}\sigma_b)^2 + (\frac{\partial f}{\partial x_{i+1}}\sigma_{x_{i+1}})^2 + (\frac{\partial f}{\partial x_{i-1}}\sigma_{x_{i-1}})^2} \approx \frac{1}{x_{i+1}-x_{i-1}}\sqrt{\sigma_a^2+\sigma_b^2} \tag{41}$$

In the last step we neglected the changes in σ_f due to the uncertainties of x_{i+1} and x_{i-1}, since they only lead to a difference in the order of 10^{-4}. Re-substitution and the assumption of $\sigma_a = \sigma_b = \sigma_p$ for each power value leads to:

$$\sigma_{p_{x_i}} = \frac{\sqrt{2}\cdot\sigma_p}{x_{i+1}-x_{i-1}} \tag{42}$$

Equation 42 shows that the errors for the first and last value, i.e. $\sigma_{p_{x_0}}$ and $\sigma_{p_{x_{end}}}$, in the profiles (figure 26) are twice as large as for the rest. This results from the calculation of the derivative at these points. Compare the denominator in equation 38 (i-th value) with the denominator in equation 39 (first value). The denominator also appears in the uncertainty at these points ($\sigma_{p_{x_0}}$ and $\sigma_{p_{x_{end}}}$), which makes it twice as large. This can also be seen in the figure 26.

4.2.2 Camera measurement

To determine the shape and position of the 10 mW laser with the camera, we captured an image of the laser profile on the S120VC for each run. Figure 27 shows the zoomed version of the image of the first run. Full versions of both images can be found in the appendix C.1 in figure 37.

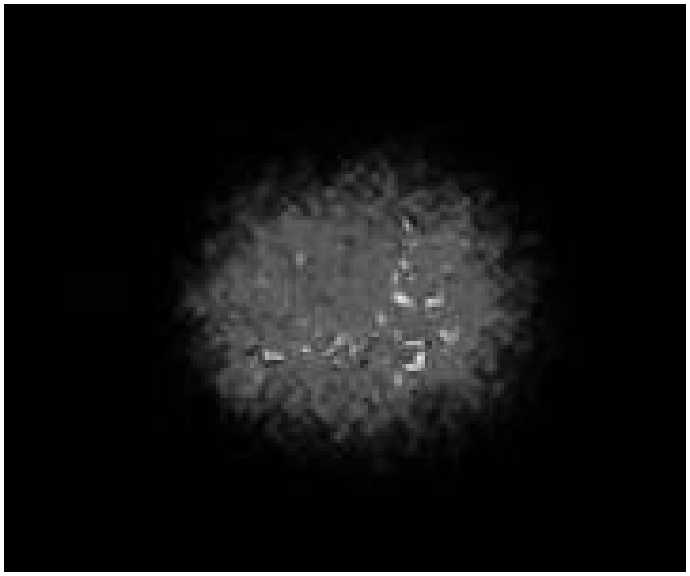

Figure 27: Zoomed image of 10 mW laser profile on the S120VC for run 1.

We arranged the pixel (of the full images) in a $m \times n$ matrix of the same size as the camera, i.e. $m \times n = 1080 \times 1920$, like:

$$(\bar{p}_{i,j})_{i=1,\dots,m;j=1,\dots,n} = \begin{bmatrix} \bar{p}_1 & \bar{p}_2 & \bar{p}_3 & \cdots & \bar{p}_n \\ \bar{p}_{n+1} & \bar{p}_{n2} & \bar{p}_{n+3} & \cdots & \bar{p}_{2\cdot n} \\ \bar{p}_{2\cdot(n+1)} & \bar{p}_{2\cdot(n+2)} & \bar{p}_{2\cdot(n+3)} & \cdots & \bar{p}_{3\cdot n} \\ \vdots & \vdots & \vdots & \ddots & \vdots \\ \bar{p}_{(m-1)\cdot(n+1)} & \bar{p}_{(m-1)\cdot(n+2)} & \bar{p}_{(m-1)\cdot(n+3)} & \cdots & \bar{p}_{m\cdot n} \end{bmatrix} \tag{43}$$

To visualize the procedure of obtaining the shape and position of the laser from this matrix we will give an example. Let us assume a fictional laser profile $F(x, y)$ with an gaussian intensity distribution as given in equation 44.

$$F(x,y) = A \cdot \exp\left(-\left(\frac{(x-\mu_x)^2}{2\sigma_x^2} + \frac{(y-\mu_y)^2}{2\sigma_y^2}\right)\right) \tag{44}$$

Here, A denotes the amplitude, μ_x and μ_y the centers and σ_x and σ_y the widths. To simulate the different axes (slow and fast) of a laser diode, we choose unequal widths ($\sigma_x \neq \sigma_y$). By distributing $F(x, y)$ over a grid with size 11×17 for the values ($A = 10$, $\mu_x = 8$, $\sigma_x = 3.5$, $\mu_y = 5$, $\sigma_y = 2.5$) we get the following grid.

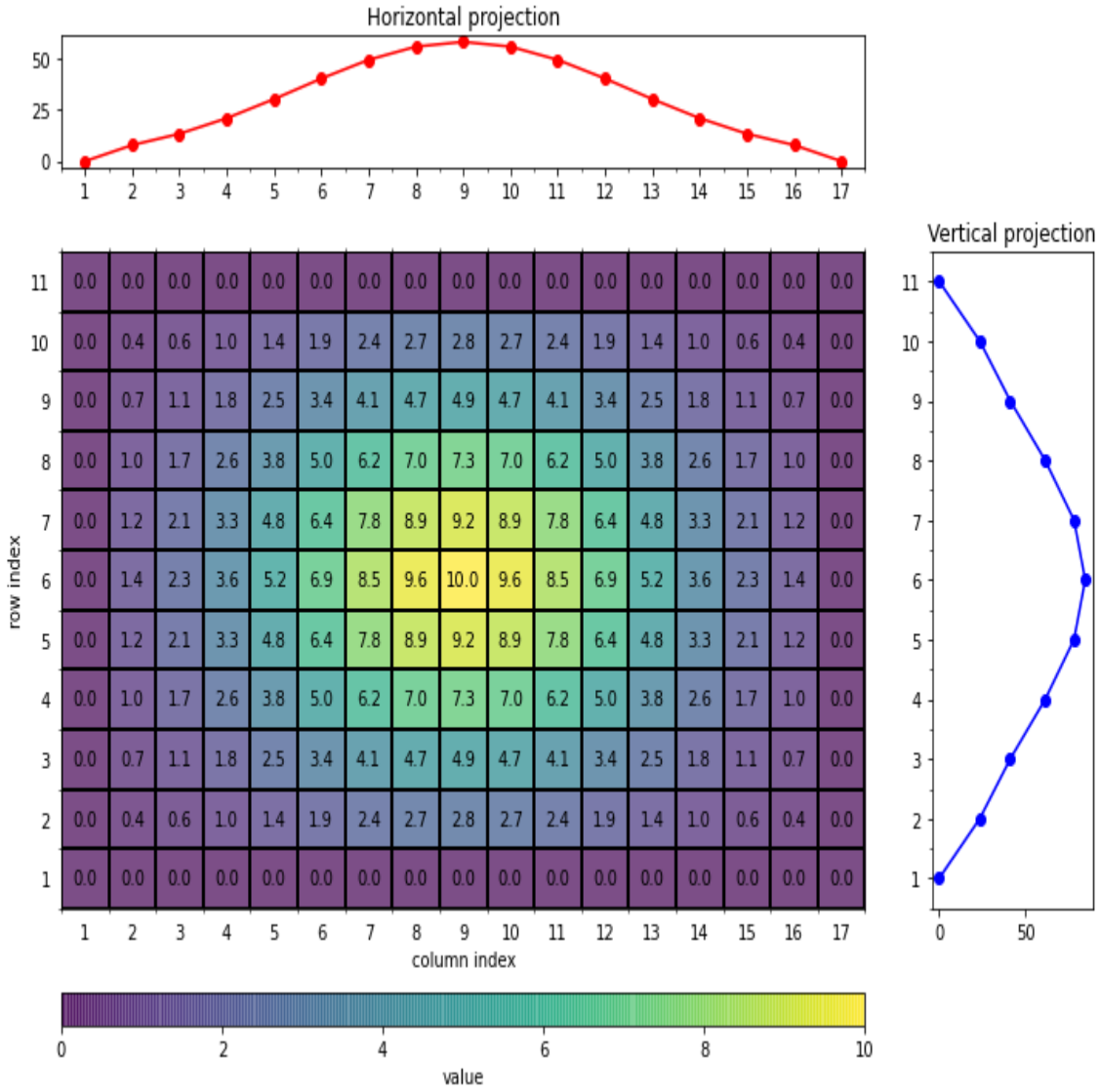

Figure 28: Horizontal (column sums) and vertical (row sums) projection of $F(x, y)$ ($A = 10$, $\mu_x = 8$, $\sigma_x = 3.5$, $\mu_y = 5$, $\sigma_y = 2.5$) distributed over a grid of the size 11×17.

Summing the values of each column (row) to one value and plotting those to their index corresponds to a horizontal (vertical) projection of $F(x, y)$. For a better overview, we give the projections in one separate plot as well (figure 29).

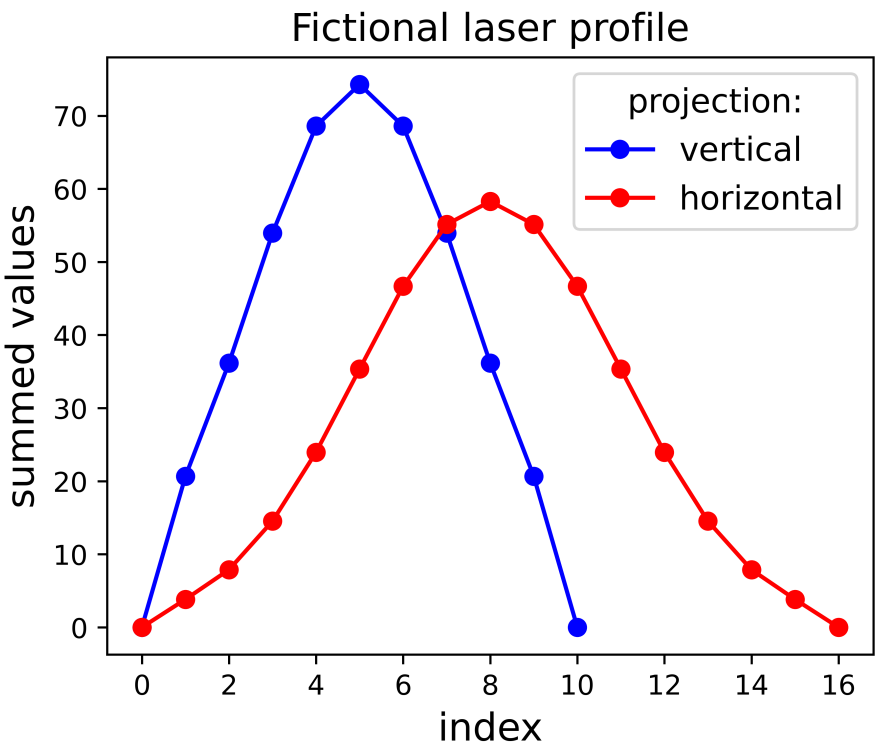

Figure 29: Horizontal (column sums) and vertical (row sums) projection of $F(x, y)$ from the grid shown in figure 28.

The results show that the horizontal (vertical) projection of $F(x, y)$ in the grid can be obtained by summing over the columns (rows). By arranging the pixels of the images captured by the camera in a matrix, we have created such a grid. Therefore, we can obtain the two projections of the 10 mW laser profile in the same way. For a better overview, we have zoomed and centred the results in figure 30. The complete and unprocessed results can be found in the appendix in the section C.1 in the figure 38.

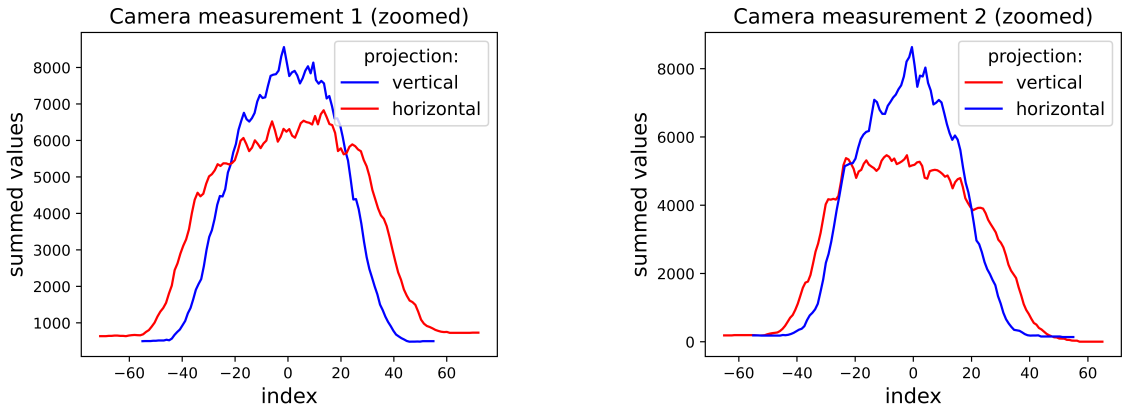

(a) (b)

Figure 30: Zoomed versions of the projections of the 10 mW laser profile on the S120VC from the camera results in figure 37 of knife-edge measurement a: 1. and b: 2. The laser diode was rotated by 90° in between the measurements.

4.2.3 Comparison between knife-edge and camera results

This is the last part of the evaluation and we will use the results (knife-edge and camera) from the two runs to compare both methods. For a better overview of the comparison, the results are given in figure 31 (figure 32) for the first (second) run.

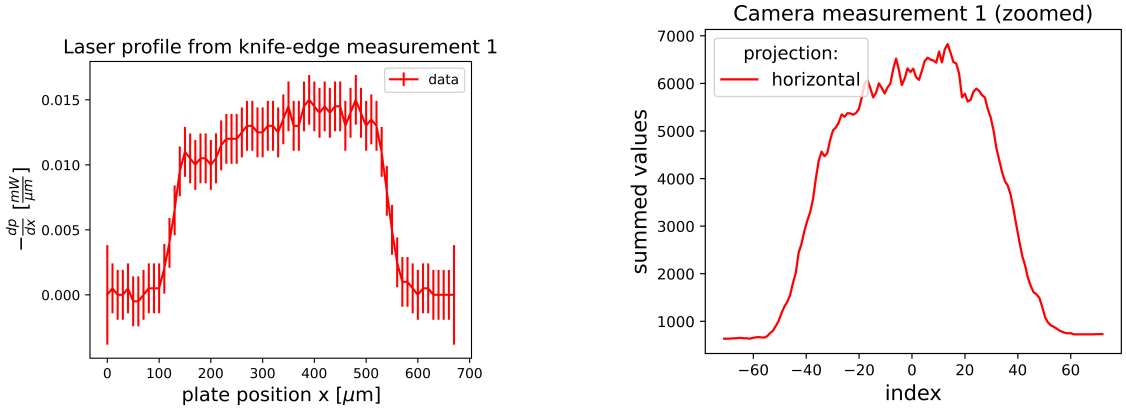

(a) (b)

Figure 31: Results for the first run. a: knife-edge. b: camera.

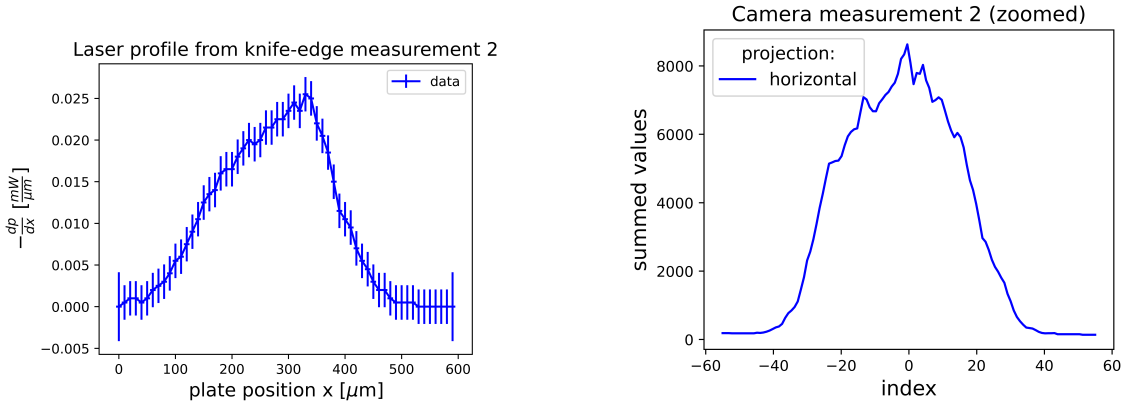

(a) (b)

Figure 32: Results for the second run. a: knife-edge. b: camera.

In order to give an estimation of the agreement between the results of the two methods, we need scale the axes to plot both in one diagram for each run. We will convert the index, i.e. pixel, of the camera results into a position with the following equation:

$$\alpha_{x_i,p_i} = \frac{\Delta x_i}{\Delta p_i} \tag{45}$$

Here, α_{x_i,p_i} and Δp denote the conversion coefficient and the pixel length of the profile from the camera result. For the first camera result, we have a pixel length of $\Delta p_1 = 133$ and for the second $\Delta p_2 = 115$. Δx denotes the distance we moved the aluminium plate into the laser beam during the knife-edge measurement. For the first knife-edge measurement we have $\Delta x_1 = 680\mu$m and for the second $\Delta x_2 = 590\mu$m. The results of the comparison are given in figure 33.

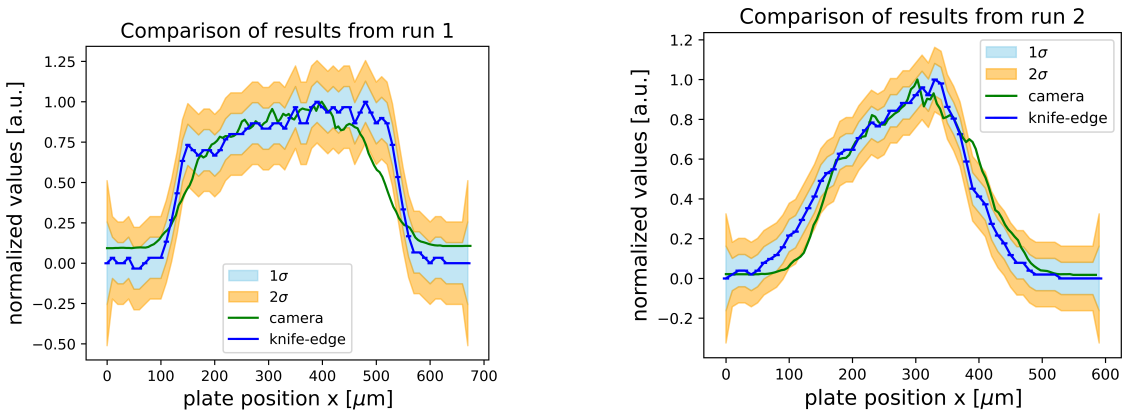

(a) (b)

Figure 33: Comparison of the data by knife-edge technique and camera for a: first run. b: second run.

The comparison shows that the results agree within the estimated errors for both projections of the 10 mW laser, which means that the camera is able to analyze the shape of the laser beam. The position can be determined by the peak (pixel position) of the horizontal and vertical projection from the camera results. We estimated the uncertainty σ_p from the knife-edge measurement to be the dominant error for the comparison and turned it into a transparent band (blue for 1σ and orange for 2σ).

To further verify the conclusion from the comparison, we compare the two conversion coefficients with each other, given in the table below:

Table 5: Conversion coefficients

axis	α $[\frac{\mu m}{pix}]$	σ_α $[\frac{\mu m}{pix}]$
horizontal	5.11	0.05
vertical	5.13	0.06

The uncertainty of the conversion coefficients has been calculated with gaussian error propagation (equation 46).

$$\sigma_{\alpha_i} = \sqrt{(\frac{1}{\Delta p_i}\sigma_{x_i})^2 + (\frac{1}{\Delta p_i}\sigma_{x_i})^2} = \frac{\sqrt{2}\cdot\sigma_{x_i}}{\Delta p_i} \tag{46}$$

The uncertainty of the position is $\sigma_{x_1} = \sigma_{x_2} = 5\mu$m. The deviation of the two coefficients is $0.26\sigma_\alpha$. From that we draw the conclusion, that both of the camera results have been converted in the same way and the statement on the comparison of the knife-edge and camera results (figure 33) is justified. The deviation was calculated with the following equation:

$$\sigma_\alpha = |\frac{\alpha_{slow} - \alpha_{fast}}{\sqrt{\sigma^2_{\alpha_{slow}} + \sigma^2_{\alpha_{fast}}}}| \tag{47}$$

5 Discussion

In this work, we characterized a Raspberry Pi NoIR v2 camera to monitor the position and shape of a laser beam on a power meter using a test setup with a 15 mW laser diode at 650 nm. This camera is intended for future use with the 2 kW laser at the CSR. The first part of this thesis involves characterizing the camera's working regime and estimating the necessary optical density (OD) filters to prevent pixel saturation for both lasers. In the second part, we measured the beam shape using the knife-edge technique and compared the results with those from the camera. The results were consistent within the error margin of the knife-edge measurement.

5.1 Working regime of the 2 kW laser and the PM3K

In order for the camera to operate within the working regime for a given setup (laser and power meter), we need to address two things. First, the intensity of individual pixel should not approach their maximum value, since then the camera observes a logarithmic response for summed pixel intensity while the power meter measures a linear response. We are sure that this is an effect of saturation, because after we decreased the intensity of individual pixel, by enlarging the laser profile on the power meter, the camera also measured a linear response for higher laser intensities. Second, the intensity should still be as high as possible, since some threshold effect of the camera seems to happen at low intensities.

Based on the intensity results for individual pixel of the camera with a filter of OD 0 (i.e. no filter) and OD 0.3 (figure 24) for the 15 mW laser diode on the MP3K, we believe that a reflective filter of OD 5.3 is necessary for the CSR setup (2 kW laser and PM3K), since the 2 kW laser is about 5 orders of magnitude stronger than the 15 mW laser. Furthermore, individual pixel for the measurement with no filter appeared to be on the edge of saturation for the highest laser power. However the effect of saturation is not yet visible in the shape of the summed intensity plots (figure 23a).

5.2 Shape and Position of a 10 mW laser on the S120VC

To demonstrate that the camera is able to monitor the beam shape and position, we determined these parameters for a 10 mW laser diode on the S120VC. We measured the beam shape with the established knife-edge method and compared the results with the recorded beam shape of the camera that was projected on one axis.

In the knife-edge method, a black anodized aluminium plate was moved horizontally through the laser beam, with a step-width of 10μm, while the 10 mW laser was held at a constant voltage of (4.50 ± 0.04) V. For each position of the plate, the power on the S120VC was recorded. After the beam was entirely blocked by the plate, we moved the plate out of the laser beam and took an image of the laser profile on the S120VC with the camera. The laser diode was then rotated by 90° by hand to determine information about the other laser axis with the knife-edge measurement. The results led to the profile of the laser beam projected onto the direction of movement of the plate (figure 26).

The shape of the two laser axes of the 10 mW laser were also determined with two images of the laser profile on the S120VC. The pixels of each image were arranged in a matrix of dimensions $1920 \cdot 1080$ and summing over the columns (rows) lead to a horizontal (vertical) projection of the laser profile from each image (figure 30).

A comparison of the results of the two methods (figure 33) showed that they agree within the uncertainty (error of the knife edge measurement). Since we did not convert the two camera results with the same conversation coefficient, we also compared the two coefficients with each other. We found a deviation of $0.26\sigma_a$, which means that both camera results were converted in a similar way and the previous statement about the quality of the comparison (knife-edge and camera) is valid. The deviation was calculated using the uncertainties of the conversion coefficients (table 5).

In our comparison of the different methods, we have not taken into account that the camera observes the S120VC at an angle of 10.3°. Furthermore, we have not taken into account that the knife-edge method measures the beam profile at a distance of 17.5 cm from the laser diode, while the camera measures the beam profile on the S120VC at a distance of 27.5 cm from the laser. Both points lead to a further error between the results of the two methods. All experimental setups in this work are placed on an optical table. Due to the size of the mounts of the individual components, the camera could not be positioned at smaller angles. The error due to the different position in the beam profile measurement however, could be eliminated if the S120VC is placed at the location of the knife-edge for the camera measurement.

Using a beamsplitter, which divides the beam into two beams of equal power, could further improve the comparison, because power fluctuations of the laser diode during the knife-edge measurement can be recorded this way. A feedback loop could then be build to ensure that the power output of the laser diode is stable over time or the knife-edge data could be corrected in the evaluation later. Another way to improve the comparison is in the knife-edge itself. Our construction is only able to move the plate in a horizontal line. We therefore had to rotate the laser diode by 90° to measure the other projection of the laser profile too. This introduces a systematic error on the shape of the laser beam between the two camera results. Leading us to only use one projection of the laser profile from each image, even though both projections can be obtained by one image. By using a knife-edge construction, which can measure two perpendicular axes of the laser profile in one run, only one image of the camera would be needed. An automatic version of the knife-edge, in which the plate is moved by electrical components would also further improve the results and thus the comparison, since a smaller step-width could be achieved leading to more measurement points and thus improvement of the quality of the data.

To summarise, however, it can be said that the camera is quite suitable for our task, namely the observation of the position and shape of the 2kW laser profile for future experiments in the CSR.

5.3 Outlook

In this work, we have estimated that the camera needs a reflective filter with an optical density of 5.3 to work with the 2 kW laser in the CSR setup. The next step is to install the camera and filter and take an image of the laser profile on the PM3K. The intensity of the individual pixels of the brightest area of the image must then be observed. This data can then be used to check if the estimated filter for the 2 kW laser in this thesis is correct.

The experimental setup we used in this work only has a small laser power range in which the camera can be operated. This is due to the fixed gain value of the camera, which is required for the pulsed operating mode of the laser. The power range could be increased by determining the gain value for different powers of the 2 kW laser required to operate the camera in working mode. This can be determined by comparing intensity measurements (at different laser powers) with a

power measurement of the 2 kW laser at the PM3K. Such an extension of the power range of the camera is not necessary for the use of the 2 kW laser at the CSR, as it is operated at constant power. However, it could open doors for other experiments and experimental setups in which the laser is mostly operated at the same power.

Appendices

A Experimental setup

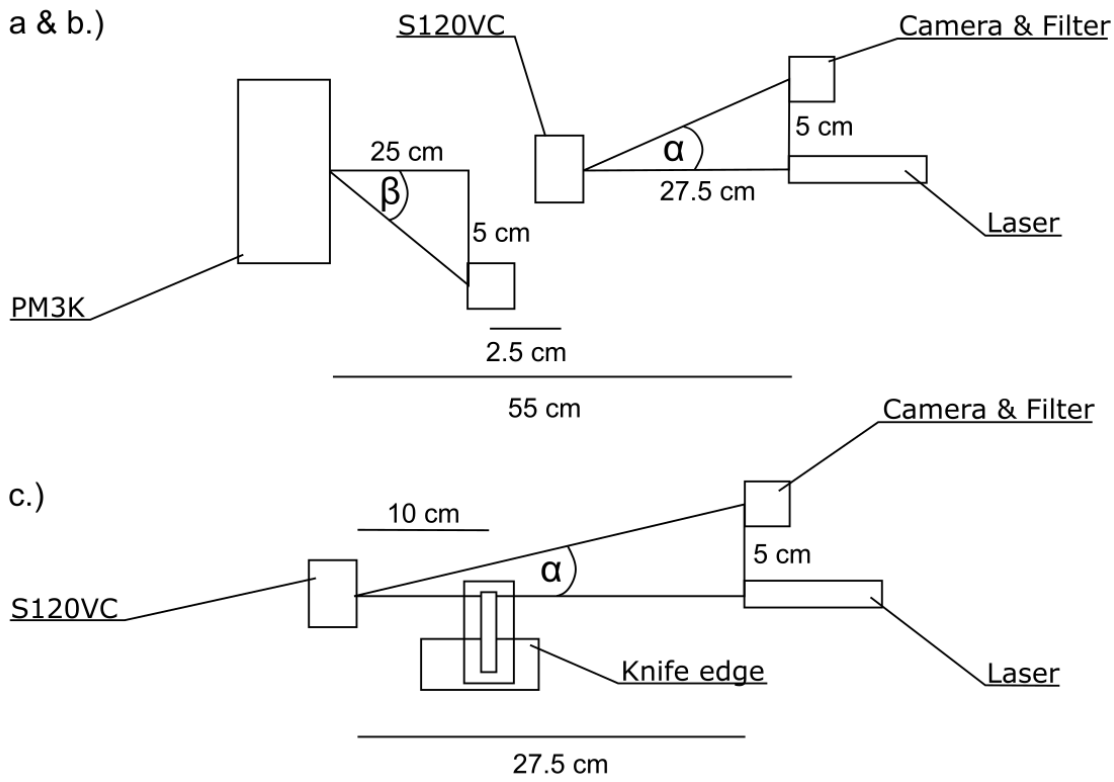

Figure 34: a.) Top view of experimental set up a/b. b.) Top view of experimental set up c. The angles between the camera and the target are $\alpha = 10.3°$ and $\beta = 11.31°$

B Working regime of the camera for 2 kW laser and the MP3K

B.1 Voltage measurement

These measurements belong to the estimation of the voltage uncertainty (chapter 4.1.1) for the power adapter used in the experiments.

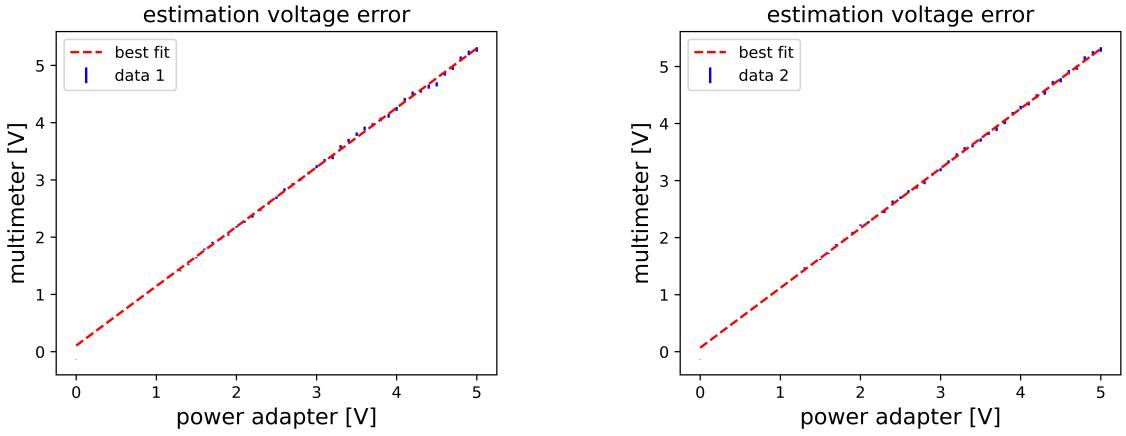

(a) (b)

Figure 35: Voltage measurement on power adpater (VLP-2403 from VOLTCRAFT) with multimeter (UT131B Multimeter from UNI-T).

Both results show a linear response. In addition, we were able to determine that the voltage values of the power adapter (VLP-2403) have a constant offset of $v_{offset} = (0.087 \pm 0.014)$ V. This value was determined as the average of the y-axis intercepts of both straight lines. We have therefore corrected our recorded power supply values $v_{powersupply}$ by $v_{offset} = 0.087$ V according to:

$$v = v_{power\ adapter} + v_{offset} \tag{48}$$

For the uncertainty $\delta v_{power\ adapter}$ of the individual voltage values $v_{power\ adapter}$ of the power supply, we have used the corresponding voltage values of the multimeter $v^1_{multimeter}$, $v^2_{multimeter}$. We have estimated the uncertainty $\delta v_{power\ adapter}$ as the difference between $v^1_{multimeter}$, $v^2_{multimeter}$:

$$\delta v_{power\ adapter} = |v^1_{multimeter} - v^2_{multimeter}| \tag{49}$$

We did this for all voltage values $v_{power\ adapter}$ and averaged the uncertainties $\delta v_{power\ adapter}$ to obtain an average uncertainty $\bar{\delta v}_{power\ adapter} = (0.0370 \pm 0.0010)$ V for each voltage value of the power adapter. The uncertainty Δv for the corrected voltage values v was then calculated using gaussian error propagation.

$$\Delta v = \sqrt{\bar{\delta} v^2_{power\ adapter} + \Delta v^2_{offset}} \tag{50}$$

The uncertainty for each corrected value is $\Delta v = 0.04$ V.

B.2 Power measurement of the 15 mW laser on the S120VC with 23% larger beam profile

This measurement belongs to the determination of the working regime of the camera for the 15 mW laser (with 23% larger beam profile) and the S120VC from chapter 4.1.1.

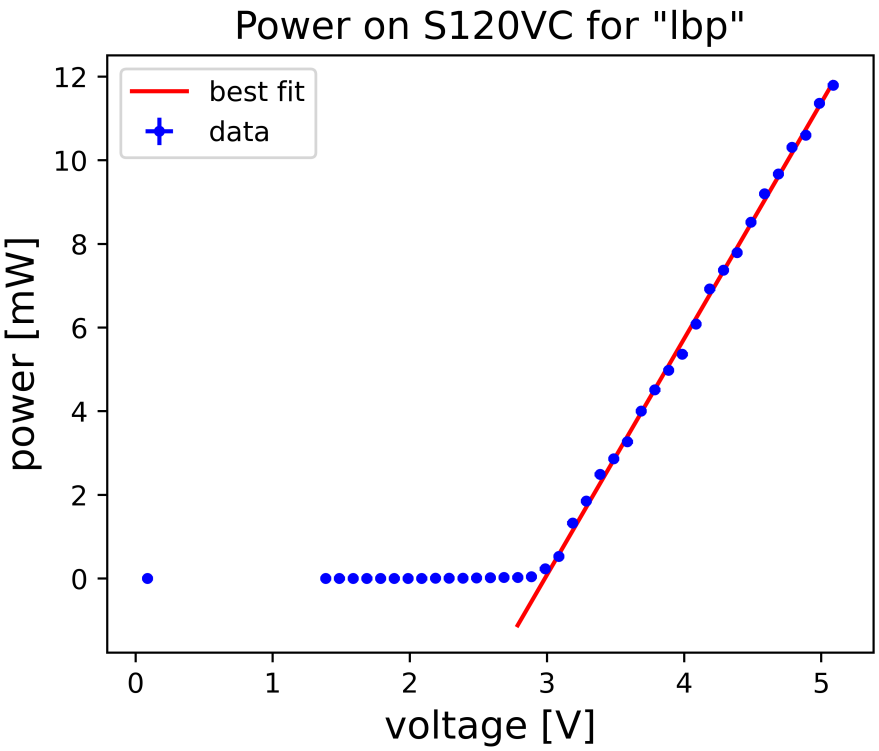

Figure 36: Power of 15 mW laser with 23% larger beam profile on S120VC

C Shape and Position of the 10 mW laser beam on the S120VC

C.1 Camera measurement

(a) (b)

Figure 37: Image of 10 mW laser profile on the S120VC for knife-edge measurement a: 1. b: 2.

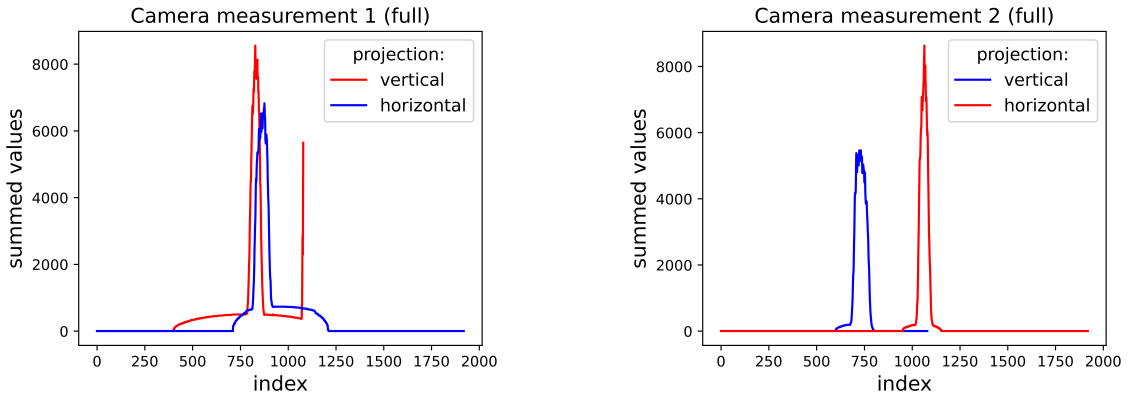

(a) (b)

Figure 38: Full versions of the projections of the 10 mW laser profile on the S120VC from the camera results (figure 37) for knife-edge measurement a: 1. b: 2.

References

[1] Arno von Hahn, R. Becker, Felix Berg, Klaus Blaum, Christian Breitenfeldt, Hisham Fadil, Florian Fellenberger, Michael Froese, Sebastian George, Jürgen Göck, et al. The cryogenic storage ring csr. *Review of Scientific Instruments*, 87(6), 2016. https://doi.org/10.1063/1.4953888.

[2] F Grussie, AP O'Connor, M Grieser, Damian Müll, A Znotins, Xavier Urbain, and H Kreckel. An ion-atom merged beams setup at the cryogenic storage ring. *Review of Scientific Instruments*, 93(5), 2022. https://doi.org/10.1063/5.0086391.

[3] Florian Grussie. Experimental studies of ion-neutral reactions under astrophysical conditions. 2016. https://hdl.handle.net/11858/00-001M-0000-002C-0BA4-8.

[4] AP O'Connor, Florian Grussie, H Bruhns, N De Ruette, TP Koenning, KA Miller, Daniel Wolf Savin, Julia Stützel, Xavier Urbain, and Holger Kreckel. Generation of neutral atomic beams utilizing photodetachment by high power diode laser stacks. *Review of Scientific Instruments*, 86(11), 2015. https://doi.org/10.1063/1.4934873.

[5] Coherent. Beamstop pm3k datasheet. *Coherent*, 2020. https://content.coherent.com/pdf/highpowerwater-cooledthermopilesensors_db25_datasheet.pdf.

[6] Albert Einstein. *Zur quantentheorie der strahlung*. Verlag u. Druck Gebr. Leemann, 1916.

[7] Wolfgang Demtröder. Experimentalphysik 3: Atome, moleküle und festkörper. pages 74–75, 215–218, 251–253, 265–267, 2016.

[8] Bahaa EA Saleh and Malvin Carl Teich. Fundamentals of photonics. pages 562–602, 2019.

[9] Joachim Heintze. Lehrbuch zur experimentalphysik band 5: Quantenphysik: Wellen, teilchen und atome. pages 42–48, 57–60, 2019.

[10] Markus Werner Sigrist. Laser: Theorie, typen und anwendungen. pages 24–43, 307–308, 352, 2018.

[11] Joachim Heintze. Lehrbuch zur experimentalphysik band 4: Wellen und optik. pages 146–148, 157–158, 2018.

[12] Joachim Heintze. Lehrbuch zur experimentalphysik band 3: Elektrizität und magnetismus. pages 154–159, 2016.

[13] Georg A Reider. Photonik: eine einführung in die grundlagen. pages 310–316, 2013.

[14] Dhruba J Biswas. A beginner's guide to lasers and their applications, part 1: Insights into laser science. pages 41–44, 300–304, 309–311, 2023.

[15] Haiyin Sun. A practical guide to handling laser diode beams. 147:1, 27–29, 2015.

[16] Raspberry Pi Ltd. Raspberry pi camera module 2 noir. *Raspberry Pi Documentation*, 2016. https://www.raspberrypi.com/products/pi-noir-camera-v2/.

[17] Photo by Jainath Ponnala. a close up of a raspberry board on a table. *unsplash*, 2021. https://unsplash.com/de/fotos/nahaufnahme-eines-himbeerbretts-auf-einem-tisch-jvHymbpto1E?utm_content=creditShareLink&utm_medium=referral&utm_source=unsplash.

[18] Raspberry Ltd. Raspberry pi documentation. *Raspberry Pi Documentation*, 2012. https://picamera.readthedocs.io/en/release-1.13/index.html.

[19] Thorlabs. Photodiode power sensor s120vc datasheet. *Thorlabs*, 2024. https://www.thorlabs.de/newgrouppage9.cfm?objectgroup_id=3328&pn=S120VC.

[20] G.E. Stutz G.F. Marshall. Handbook of optical and laser scanning. *CRC Press*, 2011.

[21] UNI-T. Ut131b multimeter. *datasheet*, 2024. https://www.clasohlson.com/medias/sys_master/9606012960798.pdf.

[22] Raspberry Pi Ltd. Raspberry pi camera module 2 noir. *Raspberry Pi Documentation*, 2016. /https://www.raspberrypi.com/documentation/computers/.